Acta Pharmaceutica Sinica B 2025;15(9):4789−4806

Chinese Pharmaceutical Association
Institute of Materia Medica, Chinese Academy of Medical Sciences

Acta Pharmaceutica Sinica B

www.elsevier.com/locate/apsb
www.sciencedirect.com

ORIGINAL ARTICLE

Palmitoylated SARM1 targeting P4HA1 promotes collagen deposition and myocardial fibrosis: A new target for anti-myocardial fibrosis

Xuewen Yang[a,g,†], Yanwei Zhang[a,†], Xiaoping Leng[d,†], Yanying Wang[a], Manyu Gong[b], Dongping Liu[a], Haodong Li[a], Zhiyuan Du[a], Zhuo Wang[d], Lina Xuan[a], Ting Zhang[c], Han Sun[a], Xiyang Zhang[a], Jie Liu[a], Tong Liu[a], Tiantian Gong[a], Zhengyang Li[a], Shengqi Liang[a], Lihua Sun[a], Lei Jiao[a,*], Baofeng Yang[a,f,*], Ying Zhang[a,e,*]

[a]*State Key Laboratory of Frigid Zone Cardiovascular Diseases (SKLFZCD), Department of Pharmacology (State Key Labratoray−Province Key Laboratories of Biomedicine−Pharmaceutics of China, Key Laboratory of Cardiovascular Research, Ministry of Education), College of Pharmacy, Harbin Medical University, Harbin 150081, China*
[b]*College of Bioinformatics Science and Technology, Harbin Medical University, Harbin 150081, China*
[c]*Department of Inorganic Chemistry and Physical Chemistry, College of Pharmacy, Harbin Medical University, Harbin 150081, China*
[d]*Department of Ultrasound Imaging, the Second Affiliated Hospital of Harbin Medical University, Heilongjiang Province, Harbin 150086, China*
[e]*Ultrasound Imaging Department of the Second Affiliated Hospital of Harbin Medical University, and State−Province Key Laboratories of Biomedicine−Pharmaceutics, College of Pharmacy of Harbin Medical University, Harbin 150081, China*
[f]*Research Unit of Noninfectious Chronic Diseases in Frigid Zone, Chinese Academy of Medical Sciences, Harbin 150081, China*
[g]*Department of Pharmacology, Institute of Pharmacokinetics and Liver Molecular Pharmacology, Baotou Medical College, Baotou 014040, China*

Received 3 July 2024; received in revised form 13 November 2024; accepted 20 December 2024

*Corresponding authors.
E-mail addresses: jiaolei116@163.com (Lei Jiao), yangbf@ems.hrbmu.edu.cn (Baofeng Yang), jennying223@hrbmu.edu.cn (Ying Zhang).
[†]These authors made equal contributions to this work.
Peer review under the responsibility of Chinese Pharmaceutical Association and Institute of Materia Medica, Chinese Academy of Medical Sciences.

https://doi.org/10.1016/j.apsb.2025.07.011

KEY WORDS

SARM1;
Post-translational modification;
Palmitoylation;
P4HA1;
Collagen synthesis;
Fibrosis after myocardial infarction;
Anti-cardiac fibrosis;
Berberine chloride

Abstract Myocardial fibrosis is a serious cause of heart failure and even sudden cardiac death. However, the mechanisms underlying myocardial ischemia-induced cardiac fibrosis remain unclear. Here, we identified that the expression of sterile alpha and TIR motif containing 1 (SARM1), was increased significantly in the ischemic cardiomyopathy patients, dilated cardiomyopathy patients (GSE116250) and fibrotic heart tissues of mice. Additionally, inhibition or knockdown of SARM1 can improve myocardial fibrosis and cardiac function of myocardial infarction (MI) mice. Moreover, SARM1 fibroblasts-specific knock-in mice had increased deposition of extracellular matrix and impaired cardiac function. Mechanically, elevated expression of SARM1 promotes the deposition of extracellular matrix by directly modulating P4HA1. Notably, by using the Click-iT reaction, we identified that the increased expression of ZDHHC17 promotes the palmitoylation levels of SARM1, thereby accelerating the fibrosis process. Based on the fibrosis-promoting effect of SARM1, we screened several drugs with anti-myocardial fibrosis activity. In conclusion, we have unveiled that palmitoylated SARM1 targeting P4HA1 promotes collagen deposition and myocardial fibrosis. Inhibition of SARM1 is a potential strategy for the treatment of myocardial fibrosis. The sites where SARM1 interacts with P4HA1 and the palmitoylation modification sites of SARM1 may be the active targets for anti-fibrosis drugs.

1. Introduction

Myocardial fibrosis, caused by a variety of heart diseases (diabetic cardiomyopathy, myocardial ischemia, myocarditis, etc.), can develop into heart failure[1-4]. During myocardial infarction (MI), the worst threat to human lives, the fibrosis process is over-activated to fill in the damaged area, and excess collagen is synthesized, therefore causing impaired cardiac function[5-7]. Thus, inhibition of collagen synthesis and maturation is becoming an important strategy for the treatment of fibrotic diseases[8].

In the clinic, nintedanib and pirfenidone, the only two FDA (U. S. Food and Drug Administration)-approved antifibrotic drugs, are used for the treatment of idiopathic pulmonary fibrosis. Among them, pirfenidone led to a significant decrease in cardiac fibrosis but failed to ameliorate diastolic dysfunction. At present, there is still a lack of targeted therapeutic drugs for delaying myocardial fibrosis, underscoring the need to discover novel targets and improve clinical outcomes in patients with fibrotic heart diseases.

SARM1 (sterile alpha and TIR motif containing 1) was widely distributed in the brain, eyes, heart, etc.[9], and showed effects on multiple diseases, especially in nervous system disease, metabolic disease, and cancer. To be more specific, SARM1 has enzymatic properties that can degrade nicotinamide adenine dinucleotide (NAD^+), which is detrimental to the nervous system[10-13]. It was reported that activation of SARM1 leads to degradation of NAD^+ and subsequent axonal degeneration[14,15]. A role for SARM1 in innate immunity activation is known. HFD-induced steatohepatitis and metabolic disorders are reduced by deletion of SARM1 through inhibition of TLR4/7/9 and nuclear factor κB (NF-κB) pathways[16]. Additionally, SARM1 acts as a downstream target of miR-124-3p in prostate cancer (PCa), promoting the growth and metastasis of PCa cells[17]. Several small molecule inhibitors targeting SARM1 have been discovered and developed in recent years, such as a series of isothiazole inhibitors[18], isoquinoline inhibitors[19], disulfiram[20], berberine chloride (BBC), zinc chloride ($ZnCl_2$)[21], etc. SARM1, consisting of 724 amino acids, contains 3 predicted domains: an N-terminal self-inhibited Armadillo/HEAT motif (ARM) domain, tandem SAM1 and SAM2 oligomerization domains, and a C-terminal catalytic TIR domain[22]. It had been known that the TIR domain was a function of catalyzing the degradation of NAD^+. Our previous study verified that NAD^+ had protective effects on MI, especially in the diabetic mice with MI[23]. We have, therefore, proposed that SARM1 may have potential regulation effects on cardiovascular diseases. While the role of SARM1 in the cardiovascular system has not been reported. So we were interested in exploring its role in cardiovascular diseases.

Recently, studies have shown that the post-translational modification of proteins plays an important role in the regulation of diseases and is also a hot spot in the development of therapeutic drug targets[24,25]. Tepmetko, approved by the FDA in 2021, is a selective mesenchymal−epithelial transition tyrosine kinase inhibitor for the treatment of solid tumors. It selectively binds to mesenchymal−epithelial transition and inhibits its phosphorylation, thereby inhibiting carcinogenesis caused by mutations in the mesenchymal−epithelial transition gene[26]. This suggests that protein post-translational modification sites have the potential to become drug targets. Palmitoylation (also known as *S*-acylation or protein palmitoylation) is a kind of post-translational modification. It affects the structure, stability, function, and localization of a protein by attaching palmitoyl groups to specific cysteine residues of the protein[27]. Palmitoylation is essential in cell proliferation, cell differentiation, apoptosis and autoimmunity[28-30]. The process of palmitoylation is mediated by the zinc finger DHHC-type (ZDHHC) protein family (ZDHHC1−ZDHHC23). Moreover, studies have shown that palmitoylation can regulate the progression of fibrosis. CD36 palmitoylation promotes hepatic fibrosis in mice with nonalcoholic steatohepatitis[31]. A recent study suggests that small-molecule STING (stimulator of interferon genes) palmitoylation inhibitors attenuate the development of ischemic heart failure[32]. However, the role of palmitoylation in the regulation of myocardial fibrosis after MI is largely unknown. Whether palmitoylation sites are promising drug targets still needs to be explored.

After MI, a large amount of extracellular matrix is deposited in the infarcted area, causing the heart structural remodeling, thus inducing cardiac dysfunction. Collagen is the principal component of this extracellular matrix. Collagen triple helix stability depends

on the hydroxylation of proline residues by 4-hydroxy-prolyl hydroxylase (C−P4H)[33,34]. The P4H holoenzyme consists of 3 subtypes of the P4HA enzyme (P4HA1, P4HA2, and P4HA3), as well as P4HB, producing P4H1, P4H2 and P4H3 enzymes based on their composition[35]. P4HA1 promotes collagen synthesis and accelerates cancer fibrosis, thereby accelerating tumor metastasis[36,37]. In addition, studies have shown that P4HA1 is highly correlated with atrial fibrillation[38], and atrial fibrosis is an important pathophysiological factor in atrial fibrillation[39]. Consequently, the role of P4HA1 in myocardial fibrosis after MI needs further clarification.

In the present study, we identified a previously unrecognized role of SARM1 in myocardial fibrosis. SARM1 protein level was increased in the fibrotic heart and SARM1 deficiency attenuates cardiac dysfunction and remodeling in MI mice. Based on the fibrosis-promoting effect of SARM1, we screened several drugs with anti-myocardial fibrosis activity including disulfiram, BBC, 5-iodoisoquinoline (DSRM-3716), $ZnCl_2$ and selonsertib. These findings establish an unrecognized role for SARM1 and P4HA1 in the regulation of cardiac fibrosis and provide new therapeutic targets for cardiac fibrosis.

2. Materials and methods

2.1. Experimental animals

Eight-week-old male mice (C57BL/6) weighing 21−25 g were obtained from Liaoning Changsheng Biotechnology Co., Ltd. (Benxi, China) and kept at a constant temperature of 22 ± 1 °C and 50% relative humidity environment with free access to food and water. The myocardial fibrosis mice model was established by blocking the left anterior descending coronary artery (LAD) for 28 days as previously reported[21]. The use of animals is approved by the Ethics Committee of Harbin Medical University (IRB3036621) and conformed to the Guidelines for the Care and Use of Laboratory Animals published by the U.S. National Institutes of Health. After MI modeling, berberine hydrochloride (BBC, HY-18258, 20 mg/kg, MCE, Monmouth Junction, NJ, USA) and selonsertib (HY-18938, 20 mg/kg, MCE) were orally administered for 7 consecutive days and continued to be raised for 28 days.

2.2. Fibroblasts-specific SARM1 knock-in mice

Fibroblasts-specific *Sarm1* knock-in mice (*Sarm1*$^{fl/fl}$/Cre) mice were generated by crossing *Sarm1*$^{fl/fl}$ mice (Cyagen Biosciences Inc., Santa Clara, CA, USA) with C57BL/6 background and placing the CreERT-IRES-hpAP (human placental alkaline phosphatase) element under the mouse Col1a2 enhancer driven Cre mice (Col1a2-CreER, Cyagen Biosciences Inc.). Tamoxifen was dissolved in corn oil and injected intraperitoneally (40 mg/kg) into each mouse for 5 consecutive days. One week later, the heart function of the mice was tested.

2.3. Cell culture and treatment

Healthy C57BL/6 newborn mice (within 3 days after birth) were provided by the Animal Center of the Second Affiliated Hospital of Harbin Medical University. Neonatal mouse cardiac fibroblasts (NMCFs) were isolated from mouse hearts with trypsin−EDTA solution (Beyotime, Shanghai, China) and cultured with DMEM (Hyclone, Logan, Utah, USA), which contained 10% fetal bovine serum (FBS, Biological Industries, Kibbutz Beit Haemek, Israel), penicillin (100 U/mL)/streptomycin (0.1 mg/mL) (Beyotime). The cells were incubated at 37 °C in humidified air containing 5% CO_2 and 95% N_2. The NMCFs were treated with TGF-β1 (10 ng/mL, 100-21-10UG, PeproTech, Cranbury, NJ, USA) for 48 h to induce fibrosis model and use BBC (HY-18258, MCE), disulfiram (HY-B0240, MCE), 5-iodoisoquinoline (DSRM-3716, HY-W021879, MCE) and zinc chloride ($ZnCl_2$, 7646-85-7, Aladdin, Shanghai, China) to evaluate its impact on fibroblast activation *in vitro*.

2.4. Plasmid and siRNA transfection

Normal *Sarm1* plasmids, mutant SARM1 (C13S, C350S, C13S/C350S) plasmids and plasmids for knocking down SARM1 (Sh-*Sarm1*) were generated by VectorBuilder (Guangzhou, China). An empty vector was used as a negative control. All plasmids have been sequenced to confirm accuracy without necessary mutations. According to the manufacturer's description, small interference (si)RNA si*P4ha1*—CCATGAACGTGGACAAGAA, si*Zdhhc3*—GGACCCAAGTACACTCCAT, si*Zdhhc9*—GGAACTACCGCTACTTCTA, si*Zdhhc16*—TAGGAATCCTTACAACTAT, si*Zdhhc17*—GTGTCAGCTGTACCAGATA, si*Zdhhc21*—CCTGGAAGACTCCCTGAAA (RiboBio Co., Ltd., Guangzhou, China) was transfected into NMCFs. The transfection efficiency was verified by qRT-PCR.

2.5. Virus vector construction and infection

In this study, the adeno-associated virus (AAV) was used as vectors to infect heart tissue. In short, AAV9 (Postn-promoter-*Sarm1*) carrying the periostin promoter targeting fibroblasts that drives shRNA targeting *Sarm1* expression was constructed by Shanghai Genechem Co., Ltd. (Shanghai, China). AAV9-postn-promoter-*Sarm1* (VP-sh*Sarm1*) or AAV9-postn-promoter-shScramble (VP-shNC) was injected into the tail vein of mice (2×10^{11} GC vg). One week after injection, mice were exposed to MI.

2.6. Echocardiographic measurements

Four weeks after MI, cardiac function was measured by transthoracic echocardiography using the Vevo2100 high-resolution imaging system (VisualSonics, Toronto, Canada). Left ventricular ejection fraction (EF) and shortening fraction (FS) were analyzed to evaluate cardiac function.

2.7. Masson's trichrome staining

The cardiac tissue was collected and fixed in 4% paraformaldehyde for 24 h, embedded in paraffin, and cut into 5 sections along the center of the fibrotic scar with 5 μm thick. Masson trichromatic staining kit (Solarbio, Beijing, China) was used to stain the cardiac tissue. The blue color represents fibrotic tissue, and the red color represents myocardial tissue. The fibrosis area was calculated with Image Pro Plus (Media Cybernetics, Bethesda, Rockville, MD, USA). Fibrous tissue (blue area) and myocardial tissue (red area) and fibrosis area (percentage of blue area) are used to analyze the percentage of cardiac fibrosis area.

2.8. Cell counting kit-8 assay (CCK8)

CCK8 (CK04-500T; Dojindo Laboratories Inc., Kumamoto, Japan) was used to determine the cell survival rate under various

conditions. The mixture containing DMEM and CCK8 (DMEM: CCK8 = 10:1) was added into NMCFs and incubated for 1−4 h. The absorbance at 450 nm was measured by microplate reader (ABP00380, SpectraMax, Sunnyvale, CA, USA).

2.9. EdU fluorescence staining

The cell-light EdU Apollo488 *in vitro* kit (RiboBio) was used to detect newly synthesized DNA in NMCFs. All procedures are carried out following the manufacturer's instructions. In short, cells were incubated in EdU contained medium (10 μmol/L) for 4 h, fixed with 4% paraformaldehyde (Biosharp, Hefei, China), and then penetrated by 0.5% Triton X-100 (Biosharp). Cells were incubated with a dye reaction mixture, and the nucleus was stained with DAPI solution. Images were captured using a fluorescence microscope (Zeiss, Jena, Germany) and the fluorescence intensity was calculated with Image Pro Plus (Media Cybernetics, Bethesda).

2.10. Wound healing assay

The migration ability of cardiac fibroblasts was measured by the wound healing assay. After proper treatment, scrape the cells in the cell culture plate with the tip of the pipette. The floating cells were washed with PBS and the remaining cells in the culture plate continued to culture 24 h. The IX51-A12PH light microscope (Olympus, Tokyo, Japan) was used to take images of the cultured cells at 0 and 24 h. Image Pro Plus (Media Cybernetics, Bethesda) was used to calculate the cell migration rate.

2.11. Quantitative real-time PCR (qRT-PCR)

Total RNA samples were extracted from NMCFs or cardiac tissue (left ventricular peri-infarction area from MI mice and left ventricular heart tissue from sham mice) using Trizol reagent (Invitrogen, Carlsbad, CA, USA). The total RNA was converted into cDNA using the ReverTra ace qPCR RT kit (TOYOBO, Osaka, Japan). GAPDH is used as internal reference. The primer was synthesized by Sangon Biotech (Shanghai, China). Sequences for qPCR primers are listed in Table 1.

2.12. Western blot

NMCFs or cardiac tissue from the left ventricular of mice were extracted with total protein from RIPA lysis buffer (Beyotime). The protein was separated by electrophoresis on SDS-PAGE, transferred to the nitrocellulose membrane (Millipore, Billerica, MA, USA), sealed by 5% skimmed milk, and then incubated overnight with antibodies including SARM1 (YN2488, ImmunoWay, Suzhou, China), P4HA1 (66101-1-Ig, Proteintech, Rosemont, IL, USA), Collagen I (AF7001, Affinity, Cincinnati, OH, USA), Collagen III (AF5457, Affinity), α-SMA (YT5053, ImmunoWay), ZDHHC17 (YN1828, ImmunoWay) at 4 °C. The membrane was then conjugated with the second anti-rabbit or anti-mouse (LI-COR, Lincoln, NE, USA) polyclonal antibody. The protein expression level was detected and quantified by the Odyssey infrared scanning system (LI-COR). And Odyssey v1.2 software was used for analysis.

2.13. Co-immunoprecipitation/MS

Co-IP and MS were used to identify SARM1-coupled proteins. Cells were transfected with *Sarm1* overexpression plasmid. After 48 h, the cells were washed twice with PBS, and the cells were lysed with cell lysis buffer (RIPA:PI = 100:1). After ultrasound, centrifugation, extract the supernatant, and determine the protein concentration. Adopt Pierce co-immunoprecipitation (Co-IP) kit (26149, Thermo Scientific, Waltham, MA, USA) carried out Co-IP experiment (SARM1; D2M5I, Cell Signaling Technology, Danvers, MS, USA), SDS-PAGE experiment, and use mass spectrometer Q Exactivemass (Thermo Scientific), Dionex ultimate 3000 RSLCnano (Thermo Scientific) liquid chromatography detection of residual protein.

2.14. Click-iT identification of SARM1 palmitoylation

Click-iT palmitic acid azide (100 μmol/L, C10265, Thermo Scientific) was added to the cell culture medium, gently mixed, and then incubated for 6 h. The solution buffer containing protease and phosphatase inhibitor (1% sodium dodecyl sulfate in 50 mmol/L Tris−HCl, pH 8.0) was added to lyse the cells, and then the lysate was crushed with probe ultrasound, centrifuged at 15,000 × *g* for 5 min, and the protein concentration of the lysate was detected by bicinchoninic acid (BCA) method. The biotin alkyne (764213, Sigma−Aldrich, St Louis, MO, USA) was added to the protein sample and the reaction was conducted by Click-iT protein reaction buffer kit (C10276, Thermo Scientific). Then, the biotin−alkyne azide−palmitic protein complex was pulled down by streptavidin (#3419, Cell Signaling Technology). After washing, SARM1 was immunoblotted.

2.15. Immunofluorescence staining

NMCFs and cardiac tissue sections were fixed with 4% paraformaldehyde for 15 min, permeabilized with 0.2% Triton X-100 for 20 min, and blocked with 10% fetal bovine serum for 1 h at room temperature. Samples were then incubated with primary antibodies (Anti-SARM1: 1:250, bs-9001R, Bioss, Beijing, China; anti-P4HA1: 1:400, 12658-1-AP, Proteintech; anti-ZDHHC17:

Table 1 The primers used in qRT-PCR.

Gene name	Species	Forward sequence	Reverse sequence
Sarm1	Mouse	CATCACCCGCAAGAGGTTC	CCATAGGTGTACTGGCGGAA
P4ha1	Mouse	TCCCGTGCTAGTTGGAAACAAATGG	CATCGTGCCTGGTGCGTTAGAG
Zdhhc3	Mouse	GTCATCCTGCTCATCCTGCTGTG	TTGTTCTATGCCCGTCTCATCTGTG
Zdhhc9	Mouse	CGAGTAGTCCCAAAGCCCATCTTG	TTTCTCCCATTTCCGTGTCACCTTC
Zdhhc16	Mouse	CCACCAGACTCCACCACCTACC	GCCACAGAACTGCACAGGAACC
Zdhhc17	Mouse	CCCGTGGATGTTCTGGATGTTTCTC	TGCTTGTATCTCCTGGCGTTCATTC
Zdhhc21	Mouse	TGTCTGCTGCTGCTTACGATTGG	GTTCCGTGAGTGGCTGAGTGATC
Gapdh	Mouse	GATGCCCCCATGTTTGTGAT	GGCATGGACTGTGGTCATGAG

1:200, bs-6628R, Bioss; anti-α-SMA: 1:400, YT5053, ImmunoWay; DAPI: Biosharp; anti-Collagen I: 1:250, AF7001, Affinity) at 4 °C over-night followed by corresponding secondary antibody incubation. Co-localization was performed using a four-color multiple fluorescent immunohistochemical staining kit (abs50028, Absin, Shanghai, China). Images were captured using a confocal microscope (Cat #0972818, Olympus).

2.16. Measurement of collagen content

The culture medium of NMCFs was collected and the content of collagen was detected with the hydroxyproline assay kit (A030-1-1, Nanjing Jiancheng Bioengineering Institute, Jiangcheng, China). According to the manufacturer's instructions, the digestion solution was added to an equal volume of culture medium at 37 °C for 3 h, then Reagent I, Reagent II, and Reagent III were added respectively and a 60 °C water bath was performed for 15 min. After restoring room temperature, centrifuge at 3500 rpm (Thermo, Waltham, MA, USA) for 10 min. The absorbance at 550 nm is measured by a microplate reader (BioTek, Richmond, USA).

2.17. Molecular docking

The crystal structure of SARM1 and P4HA1 was obtained from the PDB database (https://www.rcsb.org/), and the AutoDock Vina software (http://vina.scripps.edu/) and Pyrx software (https://pyrx.sourceforge.io/) were used for protein and protein docking. The energy value (kcal/mol) of polymer represents the binding ability between 2 molecules. The lower the energy value, the more stable the binding. Pymol software was used for beautifying the docking graph.

2.18. Co-immunoprecipitation

For the determination of co-immunoprecipitation (Co-IP), cells were lysed with RIPA buffer containing protease inhibitor for 20 min on ice. The supernatant with protein incubation with the SARM1 antibody (13022S, Cell Signaling Technology) rotated at 4 °C overnight. Then, the target protein was extracted from the whole cell lysate using protein A/G magnetic beads (HY-K0202, MCE). Protein A/G magnetic bead-associated proteins were collected by placing tubes in magnetic stands, rinsing the beads with RIPA cracking buffer 5 times, and using 1 × SDS−PAGE was loaded with buffer to elute the binding protein, and Western blot analysis was performed.

2.19. Data analysis

Pooled data are presented as mean ± standard error of the mean (SEM) values and analyzed with SPSS 13.0 software. Statistical comparisons among multiple groups were performed using analysis of variance (ANOVA) followed by Dunnett's test. Student's *t*-test was carried out for comparisons between 2 groups. All statistical analyses were performed using GraphPad Prism 8, and $P < 0.05$ was taken to indicate a statistically significant difference.

3. Results

3.1. Upregulation of SARM1 expression in cardiac fibrosis

To explore the function of SARM1 in the regulating of human heart disease, we examined the expression of *SARM1* from the cardiac tissue of 14 non-failing donors (NF), 37 dilated cardiomyopathy (DCM) patients, and 13 ischemic cardiomyopathy (ICM) patients (GSE116250). As shown in Fig. 1A, compared with the NF group, the expression of *SARM1* was increased obviously in the cardiac tissue of ICM and DCM patients. It has been known that myocardial fibrosis is a common pathological feature of ICM and DCM, so we hypothesized that SARM1 has a regulatory effect on myocardial fibrosis. In order to test this hypothesis, we examined the expression of SARM1 in fibrotic heart tissue. A mouse model of MI was established and significant collagen deposition occurred in the heart after surgery for 28 days (Supporting Information Fig. S1), indicating the successful establishment of cardiac fibrosis model mice. Interestingly, we identified that the expression of SARM1 was significantly increased in the fibrotic heart tissue (Fig. 1B and C). To determine the reason for the high expression of SARM1 in fibrotic heart tissues, we examined the abundance of SARM1 in neonatal mouse cardiac myocytes (NMCMs) and NMCFs. As shown in Supporting Information Fig. S2A, the expression of SARM1 in NMCFs was higher than that in NMCMs, which indicated that the high expression of SARM1 in cardiac fibroblasts may be closely related to the development of myocardial fibrosis. Transforming growth factor-β1 (TGF-β1), a pleiotropic cytokine, can promote a variety of fibrotic diseases[40]. Our experiments were conducted with cultured NMCFs and generated data showing a significant increase in SARM1 level after treatment with TGF-β1 (10 ng/mL) (Fig. 1D and E). This data also indicated that SARM1 is distributed in both cytoplasm and nucleus and the TGF-β1 treatment did not cause changes in *Sarm1* mRNA levels (Fig. 1E, Fig. S2B).

3.2. Knockdown of SARM1 attenuates myocardial fibrosis

A question we wonder was whether the upregulation of SARM1 in MI is a contributor to myocardial fibrosis. To clarify this issue, we first constructed the adeno-associated virus serotype 9 vector carrying a *Sarm1*-shRNA fragment (AAV9-Postn-promoter-sh*Sarm1*, VP-sh*Sarm1*) targeting fibroblasts to knock down SARM1. The knockdown efficiency of VP-sh*Sarm1* was verified by Western blot. As shown in Fig. 1F, comparing with MI mice, the expression of SARM1 was significantly decreased in the VP-sh*Sarm1* administrated MI mice. What's more, SARM1 knockdown significantly improved MI-induced cardiac dysfunction (Fig. 1G). Furthermore, knockdown of SARM1 reduced the heart weight/body weight ratio and improved the survival rate of MI mice (Fig. 1H, Supporting Information Fig. S3). Collagen deposition is an important pathological feature of myocardial fibrosis. We examined the effect of SARM1 knockdown on collagen deposition in the heart tissue of MI mice. As depicted in Fig. 1I, VP-sh*Sarm1* significantly reduced the collagen deposition in the MI mice, while the negative control construct VP-shNC (AAV9-Postn-promoter-shNC, VP-shNC) failed to affect the collagen deposition. In addition, we further demonstrated that SARM1 knockdown can inhibit collagen deposition in myofibrotic tissue by using the hydroxyproline assay kit (Fig. 1J). Moreover, our results demonstrated that the expression of Collagen I, Collagen III and α-SMA was increased obviously in the cardiac tissue of a mouse model of myocardial fibrosis. These deleterious effects were nearly abolished by VP-sh*Sarm1* to knock down SARM1, while they are unaltered in the VP-shNC group (Fig. 1K−M).

To further clarify the effects of SARM1 knockdown on cardiac fibrosis *in vitro*, we constructed the knockout plasmid of *Sarm1* and tested its efficiency in NMCFs (Fig. 2A and B). As expected,

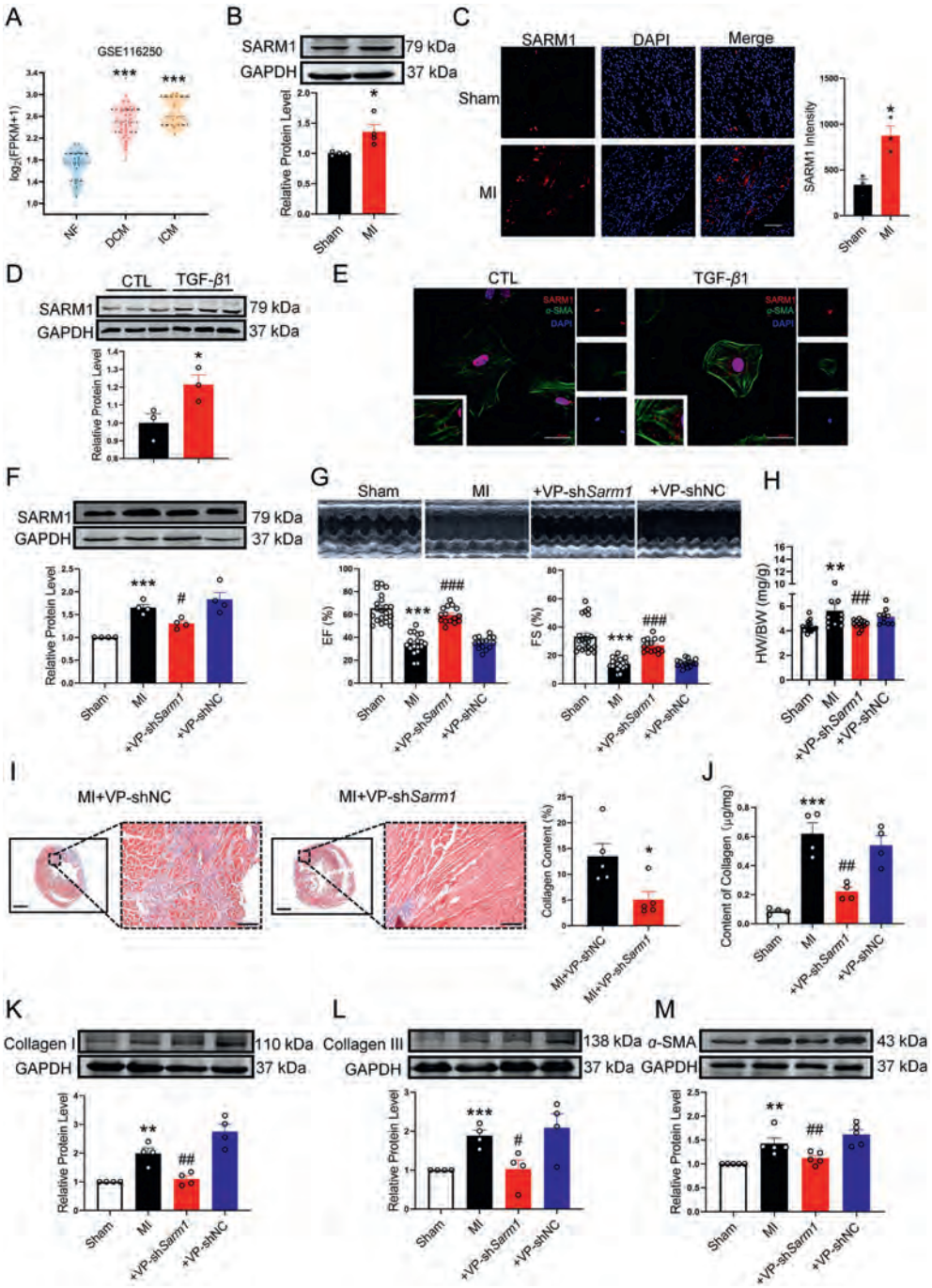

Figure 1 SARM1 upregulated expression in cardiac fibrosis, and knockdown of SARM1 attenuates myocardial fibrosis. (A) GEO datasets analyzed the differential expression of *SARM1*. (B) Western blot was used to detect the protein expression of SARM1 in the heart tissue of MI mice. $n = 4$. $^{*}P < 0.05$ *vs*. Sham. (C) Immunofluorescence was used to determine the expression of SARM1 in the heart tissue of MI mice. $n = 3$. $^{*}P < 0.05$ *vs*. Sham. Scale bar, 200 μm. (D) Western blot is used to detect the expression of SARM1 in neonatal mouse cardiac fibroblasts (NMCFs) after TGF-β1 (10 ng/mL) treatment. $n = 3$. $^{*}P < 0.05$ *vs*. CTL. (E) Immunofluorescent staining to detect the expression and localization of SARM1 in NMCFs after TGF-β1 treatment. $n = 3$. Scale bar, 400 μm. (F) Western blot was used to detect the protein level of SARM1 after tail vein injection of SARM1 knockdown virus. $n = 4$. $^{***}P < 0.001$ *vs*. Sham, $^{\#}P < 0.05$ *vs*. +VP-shNC. (G) Echocardiographic detection of cardiac function changes. $n = 15$–21. $^{***}P < 0.001$ *vs*. Sham, $^{\#\#\#}P < 0.001$ *vs*. +VP-shNC. (H) The effects of SARM1 knockdown on the heart weight/body weight ratio of mice. $n = 10$–16. $^{**}P < 0.01$ *vs*. Sham, $^{\#\#}P < 0.01$ *vs*. +VP-shNC. (I) Masson staining was used to detect the deposition of collagen in the heart tissue of mice after MI. $n = 5$. $^{*}P < 0.05$ *vs*. MI + VP-shNC. Scale bar, 1 mm (left), scale bar, 100 μm (right). (J) The hydroxyproline assay kit is used to detect the secretion of collagen in mouse heart tissue. $n = 4$. $^{***}P < 0.001$ *vs*. Sham, $^{\#\#}P < 0.01$ *vs*. +VP-shNC. (K–M) Western blot is used to detect the content of Collagen I ($n = 4$), Collagen III ($n = 4$), and α-SMA ($n = 5$) in the cardiac tissue. $^{**}P < 0.01$, $^{***}P < 0.001$ *vs*. Sham, $^{\#}P < 0.05$, $^{\#\#}P < 0.01$ *vs*. +VP-shNC. Data are presented as mean ± SEM.

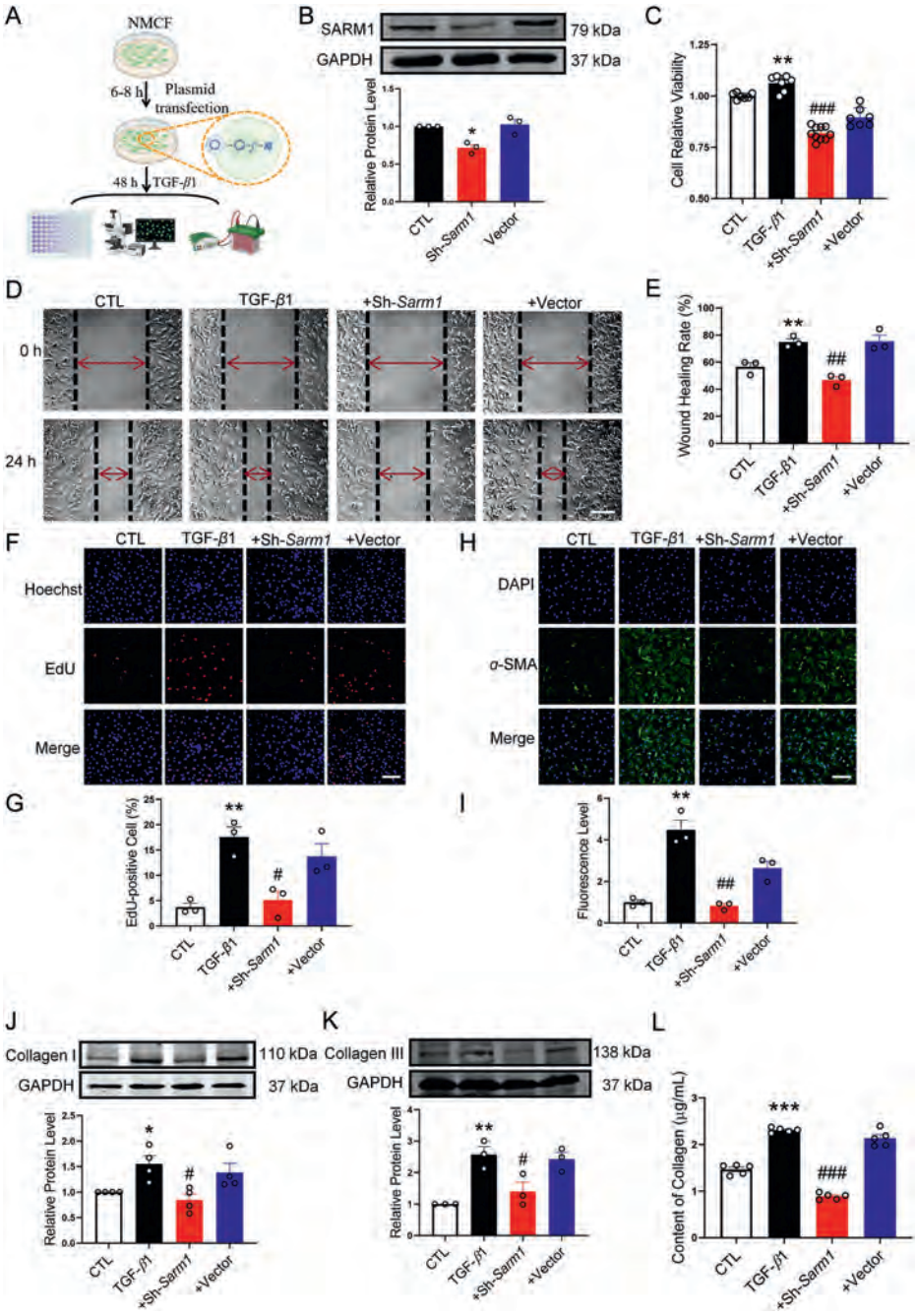

Figure 2 Knockdown of SARM1attenuates TGF-β1 induced fibrosis in NMCFs. (A) Experimental flow chart. (B) Western blot was used to detect the efficiency of SARM1 knockout plasmid (Sh-*Sarm1*). $n = 3$, $^{*}P < 0.05$ *vs*. Vector. (C) CCK8 to detect the effect of cell viability. $n = 7-9$. $^{**}P < 0.01$ *vs*. CTL, $^{\#\#\#}P < 0.001$ *vs*. +Vector. (D, E) Wound healing assay to detect the effect of cell migration ability. $n = 3$. $^{**}P < 0.01$ *vs*. CTL, $^{\#\#}P < 0.01$ *vs*. +Vector. Scale bar, 100 μm. (F, G) EdU staining was used to detect the effect of cell proliferation. $n = 3$. $^{**}P < 0.01$ *vs*. CTL, $^{\#}P < 0.05$ *vs*. +Vector. Scale bar, 200 μm. (H, I) Application of immunofluorescence in the determination of fibrosis-related protein expression of α-SMA. $n = 3$, $^{**}P < 0.01$ *vs*. CTL, $^{\#\#}P < 0.01$ *vs*. +Vector. (J, K) Western blot was used to detect the protein expression of Collagen I ($n = 4$) and Collagen III ($n = 3$) in fibroblasts. $^{*}P < 0.05$, $^{**}P < 0.01$ *vs*. CTL, $^{\#}P < 0.05$ *vs*. +Vector. (L) The hydroxyproline assay kit is used to detect the secretion of collagen. $n = 5$. $^{***}P < 0.001$ *vs*. CTL, $^{\#\#\#}P < 0.001$ *vs*. +Vector. Data are presented as mean ± SEM.

the TGF-β1 treated NMCFs had elevated cell viability, migration ability, and cell proliferation ability. These effects of TGF-β1 were effectively reversed by Sh-*Sarm1* and the negative control vector was unable to exert any appreciable impact on cell viability, migration ability, and proliferation (Fig. 2C−G). As expected, TGF-β1 treated NMCFs showed increased expression of α-SMA, Collagen I, and Collagen III, and such an increase was abolished by Sh-*Sarm1* to silence SARM1 expression (Fig. 2H−K). Similarly, the results of the hydroxyproline assay showed that SARM1 knockdown can significantly inhibit TGF-β1-induced NMCFs collagen secretion. On the contrary, the negative control vector did not elicit any significant changes (Fig. 2L).

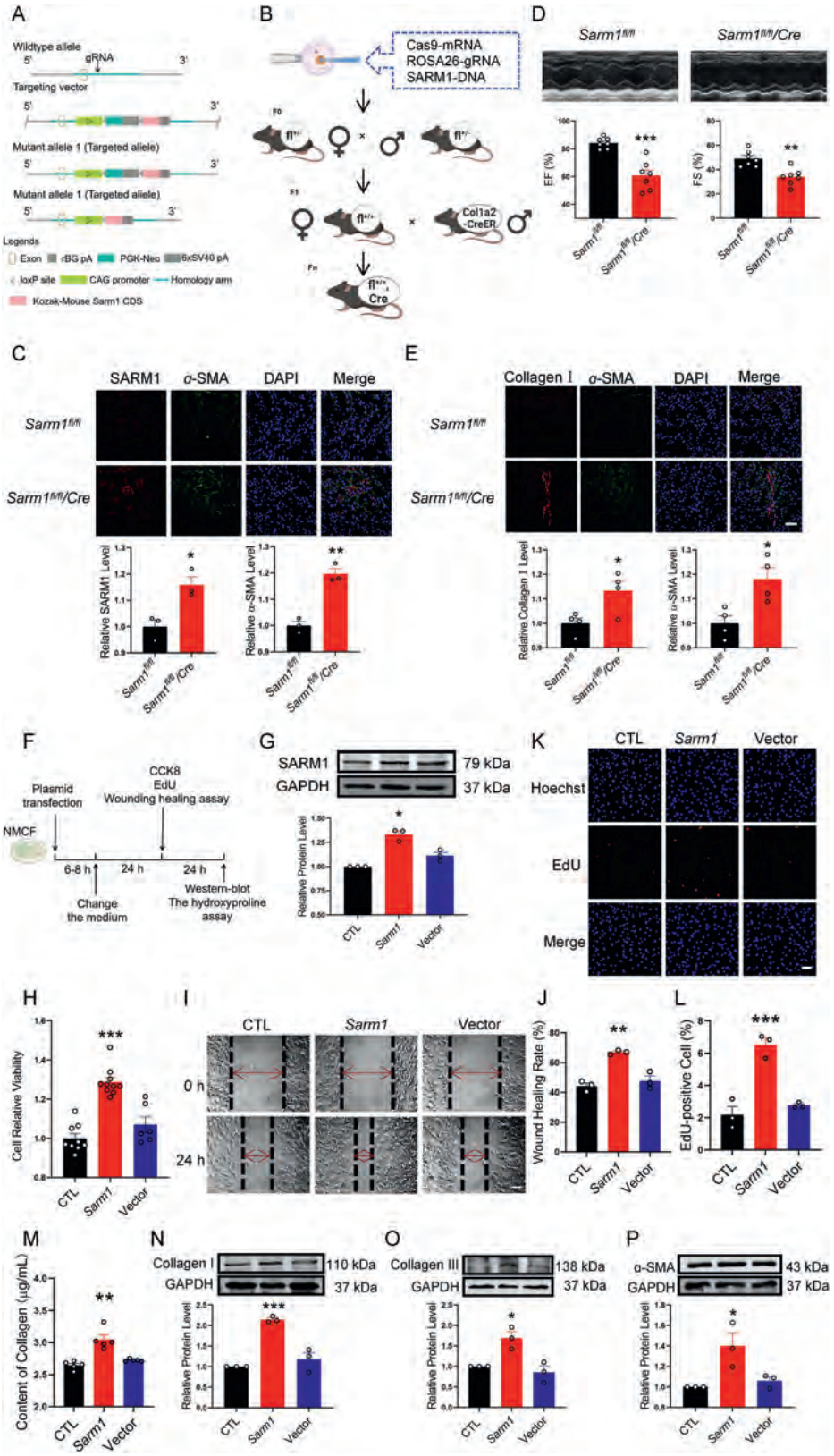

Figure 3 SARM1 overexpression aggravates cardiac fibrosis. (A) A schematic diagram of the generation of fibroblasts-specific *Sarm1* knock-in mice. (B) Reproduction diagram of transgenesis mice. (C) Immunofluorescent staining to detect the protein expression of SARM1 in myocardial fibroblasts. $n = 3$. $^{*}P < 0.05$, $^{**}P < 0.01$ *vs*. $Sarm1^{fl/fl}$. Scale bar, 200 μm. (D) Echocardiographic detection of cardiac function changes. $n = 7$. $^{**}P < 0.01$, $^{***}P < 0.001$ *vs*. $Sarm1^{fl/fl}$. (E) Immunofluorescent staining to detect the protein expression of Collagen I. $n = 4$. $^{*}P < 0.05$ *vs*. $Sarm1^{fl/fl}$. Scale bar, 200 μm. (F) Experimental flow chart. (G) Western blot was used to detect the efficiency of *Sarm1* overexpression plasmid

The results of both *in vivo* and *in vitro* studies indicate that knockdown of SARM1 reduced MI-induced myocardial fibrosis and it may also play an important role in influencing fibroblast collagen deposition in the infarct area after MI.

3.3. SARM1 overexpression aggravates cardiac fibrosis

The data above suggested that the knockdown of SARM1 reduced MI-induced myocardial fibrosis and upregulation of SARM1 may produce deleterious effects on the heart. To examine this notion, we constructed transgenic mice (*Sarm1*$^{fl/fl}$/Cre) that specifically overexpress SARM1 in fibroblasts (Fig. 3A and B). Immunofluorescence experiments were performed to verify the expression of SARM1 in *Sarm1*$^{fl/fl}$/Cre mouse cardiac fibroblasts. As shown in Fig. 3C, the expression of SARM1 was significantly increased in *Sarm1*$^{fl/fl}$/Cre cardiac fibroblasts compared with *Sarm1*$^{fl/fl}$ mice. The results of echocardiography showed that the EF% and FS% value of *Sarm1*$^{fl/fl}$/Cre mice were significantly reduced compared with the *Sarm1*$^{fl/fl}$ mice (Fig. 3D), but there was no significant change in the heart weight/body weight ratio (Supporting Information Fig. S4). Subsequent immunofluorescence results showed that similar to the results after MI, extracellular matrix deposition was significantly increased in SARM1 fibroblast-specific overexpression mice compared to *Sarm1*$^{fl/fl}$ mice (Fig. 3E). These results suggest that specific overexpression of SARM1 in myocardial fibroblasts impairs cardiac function by promoting extracellular matrix deposition.

Next, we conducted the following experiments with gain-of-function approaches *in vitro* (Fig. 3F). Firstly, the plasmid containing *Sarm1* was constructed, which was transfected into the NMCFs. As depicted in Fig. 3G, compared with the normal control vector, the transfection of the *Sarm1* vector significantly increased the protein level of SARM1. Overexpression of SARM1 significantly promoted the cell viability and migration ability of NMCFs (Fig. 3H−J). EdU staining experiment also obtained the similar results (Fig. 3K and L). In addition, overexpression of SARM1 significantly promoted the collagen secretion of NMCFs (Fig. 3M), and the expression of fibrosis-related proteins α-SMA, Collagen I, and Collagen III (Fig. 3N−P). While the normal control vector-treated NMCFs did not have these changes.

3.4. SARM1 targeting P4HA1 affects collagen synthesis in fibroblasts

To examine the underlying mechanism of SARM1 in the regulation of cardiac fibrosis, the sequencing of Co-IP mass spectrometry was used to explore the targeting protein of SARM1. As shown in Supporting Information Figs. S5A, 113 unique proteins were identified as differentially expressed in the SARM1 overexpressed NMCF. We conducted GO analysis and KEGG analysis with differentially expressed proteins. GO analysis showed that multiple signaling pathways related to fibrosis are activated, such as HIF-1, AMPK, and TGF beta signaling pathways. KEGG analysis indicated that differentially expressed proteins were associated with various cellular metabolisms and binding. Among them, P4HA1 is one of the most differentially expressed proteins (Fig. 4A). It has been reported that P4HA1, the key protein involved in the stability of the collagen triple helix during collagen synthesis, plays an important role in the regulation of cell proliferation and collagen synthesis in cancer[36]. Silencing of *P4ha1* inhibited cell proliferation, migration, and invasion, and promoted cell cycle arrest and apoptosis in high glucose-induced cardiac fibroblasts[41]. As previously reported, our results demonstrated that the expression of P4HA1 in NMCF was significantly higher than that in NMCMs (Fig. 4B). To determine the role of P4HA1 in TGF-β1 treated NMCF, we constructed the specific small interfering RNA (siRNA) of *P4ha1* (si*P4ha1*) to silence its expression and the efficiency was verified by qRT-PCR (Fig. 4C). As expected, knockdown of *P4ha1* can significantly inhibit the cell viability, migration, collagen secretion and the expression of Collagen I and Collagen III in TGF-β1 treated cardiac fibroblasts (Fig. 4D−H). Moreover, the protein level of P4HA1 was significantly increased in the SARM1 overexpressed NMCF (Fig. 4I). *In vivo*, we found a significant increase in P4HA1 protein expression in the heart tissue of *Sarm1*$^{fl/fl}$/Cre transgenic mice (Supporting Information Fig. S6A). On the contrary, knocking down SARM1 can significantly inhibit the protein expression of P4HA1 in the heart tissue of MI mice (Fig. S6B). This suggests that SARM1 may influence myocardial fibrosis by regulating the expression of P4HA1. To further verify the direct regulatory effect of SARM1 on P4HA1, the immunofluorescence and Co-IP experiments were conducted. As shown in Fig. 4J, by using confocal microscopy, we observed that SARM1 and P4HA1 had good co-localization. Consistently, the results of Co-IP experiment showed that SARM1 and P4HA1 had directly interacted with each other (Fig. 4K). These results prompt us to further explore the potential binding sites between SARM1 and P4HA1. By using computer-aided simulation of protein−protein docking, we identified that there are 9 most likely binding sites between these 2 proteins including Met1, Lys11, Glu60, Arg67, Glu71, Glu149, Glu189, Arg224, and Asp317 (from SARM1). By sequence alignment between rats, mice, and humans, we were surprised to find that the above potential binding sites are highly conserved in SARM1 (Fig. 4L and M). We constructed truncated mutants of *Sarm1* with different structural domains, and the Co-IP experiment show the same result (Supporting Information Fig. S7). This discovery shed light on the development of SARM1 to be the therapeutic targets of cardiac fibrosis.

3.5. Palmitoylation of SARM1 promotes its protein expression

Although the above data have indicated the role of SARM1 upregulation in causing elevated collagen secretion and the underlying downstream mechanisms in the setting of cardiac fibrosis, it remained unknown why SARM1 was upregulated in cardiac fibrosis. To clarify this issue, we focused on post-translational modification, which plays a crucial role in regulating protein function. Palmitoylation is one kind of post-translational modification, that affects protein stability, transport, and protein−protein or protein−membrane interactions. By online prediction (http://

(*Sarm1*). $n = 3$. $^{*}P < 0.05$ *vs*. Vector. (H) CCK8 to detect the effect of cell viability. $n = 6$−10. $^{***}P < 0.001$ *vs*. Vector. (I, J) Wound healing assay was used to detect the influence of cell migration ability. $n = 3$. $^{**}P < 0.01$ *vs*. Vector. Scale bar, 100 μm. (K, L) EdU staining was used to detect the effect of cell proliferation. $n = 3$. $^{***}P < 0.001$ *vs*. Vector. Scale bar, 200 μm. (M) The hydroxyproline assay kit is used to detect the secretion of collagen. $n = 5$. $^{**}P < 0.01$ *vs*. Vector. (N−P) Western blot is used to detect the protein expression of Collagen I, Collagen III, and α-SMA after overexpressing of SARM1 in NMCFs. $n = 3$. $^{*}P < 0.05$, $^{***}P < 0.001$ *vs*. Vector. Data are presented as mean ± SEM.

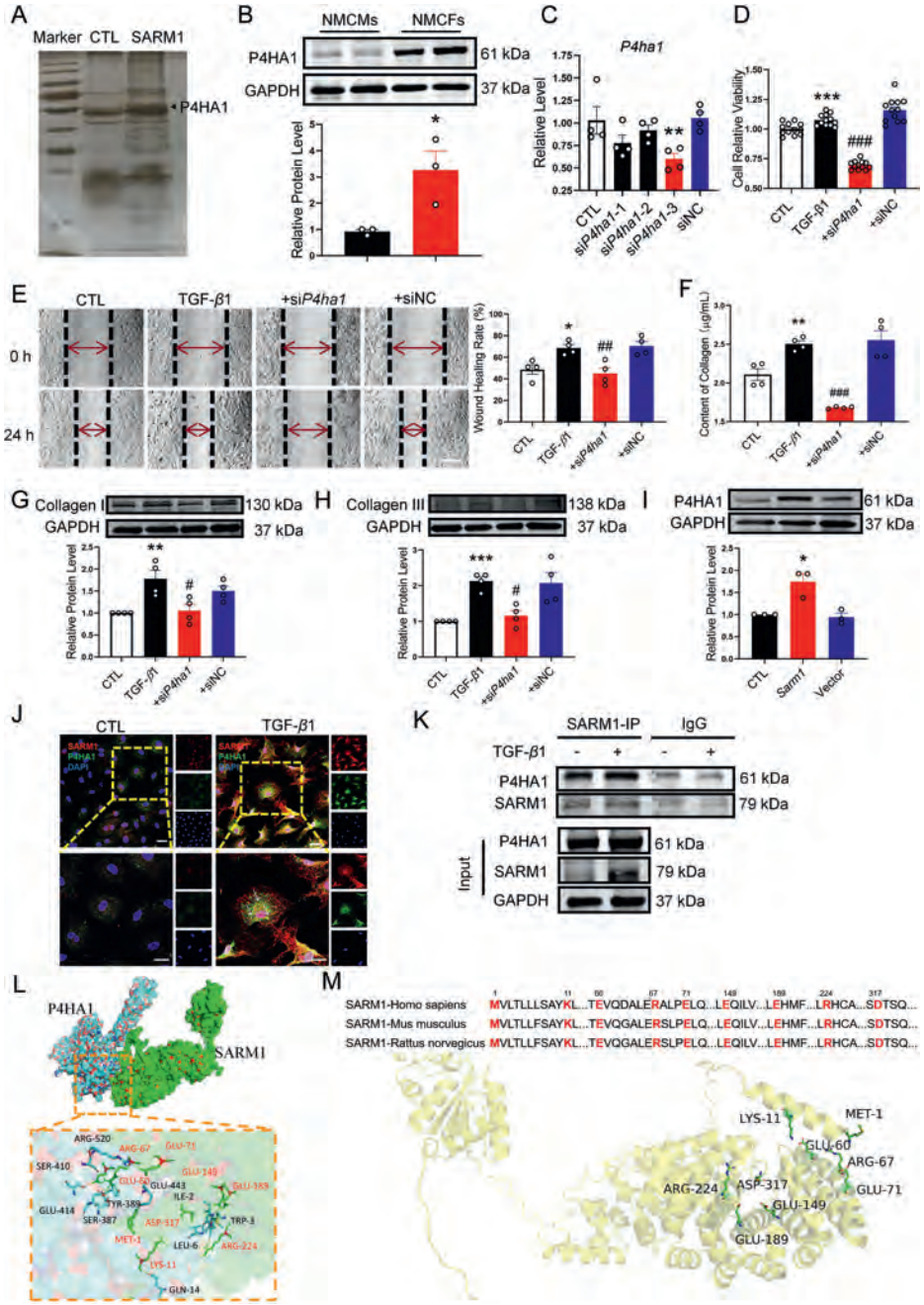

Figure 4 SARM1 targeting P4HA1 affects collagen synthesis in fibroblasts. (A) Co-IP/MS sequencing to screen the downstream effector proteins of SARM1. (B) Western blot was used to detect the expression of P4HA1 in neonatal mouse cardiac myocytes (NMCMs) and neonatal mouse cardiac fibroblasts (NMCFs). $n = 3$, $^{*}P < 0.05$ *vs*. NMCMs. (C) qRT-PCR is used to detect the knockdown efficiency of *P4ha1*. $n = 4$. $^{**}P < 0.01$ *vs*. siNC. (D) CCK8 to detect the effect of cell viability. $n = 12$. $^{***}P < 0.001$ *vs*. CTL, $^{\#\#\#}P < 0.001$ *vs*. +siNC. (E) Wound healing assay was used to detect the influence of cell migration ability. $n = 4$. $^{*}P < 0.05$ *vs*. CTL, $^{\#\#}P < 0.01$ *vs*. +siNC. Scale bar, 100 μm. (F) The hydroxyproline assay kit is used to detect the secretion of collagen. $n = 4$. $^{**}P < 0.01$ *vs*. CTL, $^{\#\#\#}P < 0.001$ *vs*. +siNC. (G, H) Western blot was used to detect the protein expression of Collagen I and Collagen III in fibroblasts after P4HA1 knockout. $n = 4$. $^{**}P < 0.01$, $^{***}P < 0.001$ *vs*. CTL, $^{\#}P < 0.05$ *vs*. +siNC. (I) Western blot was used to detect the protein expression of P4HA1 in fibroblasts after overexpression of SARM1. $n = 3$. $^{*}P < 0.05$ *vs*. Vector. (J) Immunofluorescent staining to detect the protein co-localization of SARM1 and P4HA1. Scale bars, 200 μm, 400 μm (second magnification) (K) Co-IP to detect the interaction between SARM1 and P4HA1. $n = 3$. (L, M) Molecular docking is used to predict the binding sites between SARM1 and P4HA1 by Pymol software. Data are presented as mean ± SEM.

csspalm.biocuckoo.org/online.php), we discovered that there are 2 potential palmitoylation modification sites in SARM1 including CYS13 and CYS350 and the CYS13 site had a higher score (Fig. 5A). To verify this prediction, we used Click-iT reaction to detect the palmitoylation level of SARM1 (Fig. 5B). As depicted in Fig. 5C, the palmitoylation level of SARM1 increased significantly in the TGF-β1 treated NMCF. This suggests that the palmitoylation of SARM1 may be involved in the development of

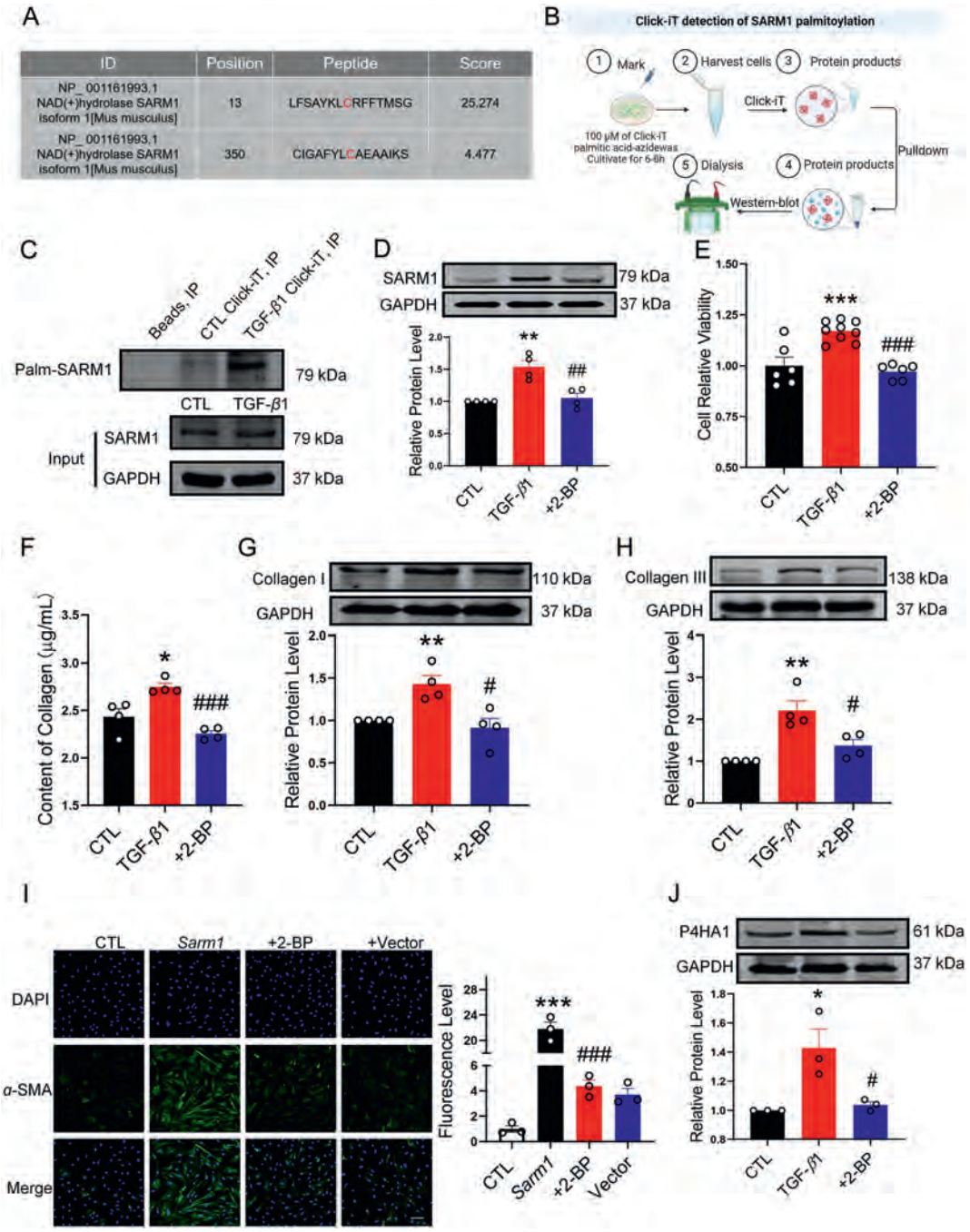

Figure 5 Palmitoylation of SARM1effects fibroblast activation. (A) Predicting the palmitoylation sites of SARM1 protein. (B) Experimental flow chart. (C) Click-iT reaction was used to detect the palmitoylation level of SARM1. $n = 3$. (D) Western blot was used to detect the protein expression of SARM1 in fibroblasts after administration of palmitoyl inhibitor (2-BP). $n = 4$. $^{**}P < 0.01$ *vs*. CTL, $^{\#\#}P < 0.01$ *vs*. TGF-β1. (E) CCK8 to detect the effect of cell viability. $n = 6-9$. $^{***}P < 0.001$ *vs*. CTL, $^{\#\#\#}P < 0.001$ *vs*. TGF-β1. (F) The hydroxyproline assay kit is used to detect the secretion of collagen. $n = 4$. $^{*}P < 0.05$ *vs*. CTL, $^{\#\#\#}P < 0.001$ *vs*. TGF-β1. (G, H) Western blot was used to detect the protein expression of Collagen I and Collagen III in fibroblasts after 2-BP administration. $n = 4$. $^{**}P < 0.01$ *vs*. CTL, $^{\#}P < 0.05$ *vs*. TGF-β1. (I) Application of immunofluorescence staining to detect the expression of α-SMA. $n = 3$. $^{***}P < 0.001$ *vs*. Vector, $^{\#\#\#}P < 0.001$ *vs*. *Sarm1*. Scale bar, 200 μm. (J) Western blot was used to detect the protein expression of P4HA1 in fibroblasts after 2-BP administration. $n = 3$. $^{*}P < 0.05$ *vs*. CTL, $^{\#}P < 0.05$ *vs*. TGF-β1. Data are presented as mean ± SEM.

myocardial fibrosis. To confirm this issue, 2-BP (50 μmol/L), a palmitoylation modification inhibitor, was used, and the results of Western blot experiment showed that inhibition of palmitoylation modification significantly reduced the protein level of SARM1 in TGF-β1 treated NMCFs (Fig. 5D). Additionally, we found that inhibition of palmitoylation modification can significantly rescue the abnormal cell viability and collagen deposition induced by TGF-β1 in NMCF (Fig. 5E−H). Furthermore, administration of 2-

BP inhibited the expression of fibrosis-related protein α-SMA in the SARM1 stimulated NMCF (Fig. 5I). Notably, inhibition of palmitoylation modification by 2-BP not only reduced the expression of SARM1 but also decreased the level of its downstream protein P4HA1 in TGF-β1 treated NMCFs (Fig. 5J).

We used palmostatin B (5 μmol/L), a depalmitoylation inhibitor (APT-1, APT-2 inhibitor) to inhibit the depalmitoylation of SARM1. The results showed that enhanced palmitoylation significantly increased the protein expression of SARM1 (Supporting Information Fig. S8A). Consistently, enhancing palmitoylation modification can also produce a similar effect as overexpressing SARM1, significantly increasing the cell migration ability and collagen secretion ability of NMCFs (Fig. S8B and S8C).

3.6. ZDHHC17 mediates palmitoylation of SARM1 in myocardial fibroblasts after MI

The above data indicated that the elevated palmitoylation level of SARM1 significantly enhanced its protein expression, thereby promoting its active involvement in fibrosis. A question we wondered was why the palmitoylation level of SARM1 was increased during cardiac fibrosis. To clarify this issue, we analyzed the subcellular localization of palmitoyltransferases based on the human protein map. We screened it by protein expression, subcellular localization, and functional loss test. First, the expression of all ZDHHC in fibroblasts was evaluated based on the human protein map (Fig. 6A). Based on the human protein profile, we found a total of 11 ZDHHC high expression in fibroblasts, of which 5 were expressed in the cytoplasm, 2 in the nucleus and 2 in the cell membrane. Since most of the palmitoylation process occurs in the cytoplasm, we further screened ZDHHC with potential regulatory effects on SARM1 through experiments, including ZDHHC3, ZDHHC9, ZDHHC16, ZDHHC17 and ZDHHC21 (Fig. 6A and B).

Then, specific siRNA was used to silence these enzymes respectively and 3 siRNAs were designed for each enzyme and their knockdown efficiency was verified by qRT-PCR (Fig. 6C). The results of the Western blot experiment showed that knocking down of *Zdhhc17* had the most significantly effects on reducing the expression of SARM1 protein (Fig. 6D). Moreover, we identified that knocking down of *Zdhhc17* reduced the palmitoylation level of SARM1 obviously in the TGF-β1 treated NMCFs (Fig. 6E). Interestingly, the mRNA level of *Zdhhc17* was obviously increased in the TGF-β1 administrated NMCFs comparing with the control group (Fig. 6F). Moreover, knocking down of *Zdhhc17* significantly inhibited cell viability and collagen secretion in the TGF-β1 treated NMCFs (Fig. 6G and H). Multiplex immunohistochemistry results showed the coexpression between ZDHHC17 and SARM1 in myocardial fibroblasts in the infarct margin area of MI tissue (Fig. 6I). The above results indicated that the increased expression of ZDHHC17 promoted the elevation of SARM1 palmitoylation levels after MI, thereby accelerating the fibrosis process.

3.7. The mutation of SARM1 in the palmitoylation site weakens its role in promoting cardiac fibrosis

A question raised was whether the SARM1 palmitoylation modification site is the key to the regulation of myocardial fibrosis. To clarify this issue, we constructed a plasmid with double mutant palmitoylation sites of *Sarm1* (C13S/C350S), replacing CYS13 and CYS350 residues with serine (S) (Fig. 7A). The level of mut-*Sarm1* was increased significantly in the *Sarm1* mutational plasmid (C13S/C350S) transfected NMCFs (Supporting Information Fig. S9A). The results of the cycloheximide (CHX) experiment showed that compared with the *Sarm1* group, the SARM1 palmitoylation double mutant group (C13S/C350S) showed a decrease in protein stability of SARM1 (Supporting Information Fig. S10). Compared with the *Sarm1* overexpression group, mutating the SARM1 palmitoylation sites significantly reduced fibroblast cell viability, collagen secretion, and cell migration (Fig. 7B−E). To further explore the effects of single palmitoylation sites CYS13 or CYS350 of SARM1 on its fibrosis promotion, we constructed single palmitoylation site (C13S, C350S) mutation plasmid of SARM1 (Fig. 7F) and verified its efficiency (Fig. S9B). Interestingly, comparing with the *Sarm1* overexpression cells, transfection of C13S mutant plasmid of *Sarm1* significantly decreased the cell viability, collagen secretion, and cell migration in NMCFs (Fig. 7G−J). On the contrary, transfection of C350S mutant plasmid of *Sarm1* had no significant influence on the cell viability and cell migration (Fig. 7G and I). The above data indicated that the palmitoylation sites of SARM1 especially CYS13, play an important role in the regulating of cardiac fibrosis and may be a potential active target for anti-myocardial fibrosis drugs.

3.8. Screening of anti-cardiac fibrosis drugs targeting SARM1

To further explore the potential role of SARM1 in translational medicine, we investigated the effects of reported SARM1 inhibitors including disulfiram, BBC, DSRM-3716, and $ZnCl_2$[18-21] on myocardial fibrosis. As illustrated in Supporting Information Fig. S11, disulfiram, BBC, DSRM-3716 and $ZnCl_2$ significantly inhibited the cell viability and collagen secretion in the TGF-β1-treated NMCFs. Moreover, we observed that disulfiram, BBC, and DSRM-3716 reduced cell viability in SARM1 overexpression NMCFs. However, $ZnCl_2$ exhibited no significant effects (Fig. 8A). Berberine has been used clinically to treat bacterial infections and various inflammatory diseases. Meanwhile, its pharmacological effects, pharmacokinetics, and adverse effects are known. In addition, studies have reported that berberine has significant inhibitory effects on fibrosis in the liver, kidney, and lung. However, the mechanism of berberine in myocardial fibrosis is still unclear. Also, we found that BBC can significantly decrease the level of collagen deposition induced by SARM1 (Fig. 8B). The above findings indicated that disulfiram, BBC, DSRM-3716, and $ZnCl_2$ may be candidates for anti-myocardial fibrosis drugs. The results of the immunofluorescence experiment showed that BBC could inhibit the expression of SARM1 (Fig. 8C). Next, we continue to explore the sites of action of the above drugs on SARM1. Using computer-assisted molecular docking technology, we found that BBC has a good binding effect on the CYS13 site of SARM1. This suggests that CYS13 has the potential to be an active site for SARM1 (Supporting Information Fig. S12).

To further evaluate the potential of SARM1 as a target for anti-cardiac fibrosis drugs, we examined the effect of selonsertib, which has entered phase III clinical trials for treating bridging fibrosis caused by nonalcoholic steatohepatitis[42] on the expression of SARM1. As shown in Fig. 8D, selonsertib can inhibit the expression of SARM1 in NMCFs. Particularly, selonsertib can significantly reduce cell viability and collagen deposition in the *Sarm1* overexpressed NMCFs (Fig. 8E and F). These data indicated that selonsertib may have effects on the MI-induced cardiac fibrosis. To verify this speculation, we constructed a mouse model

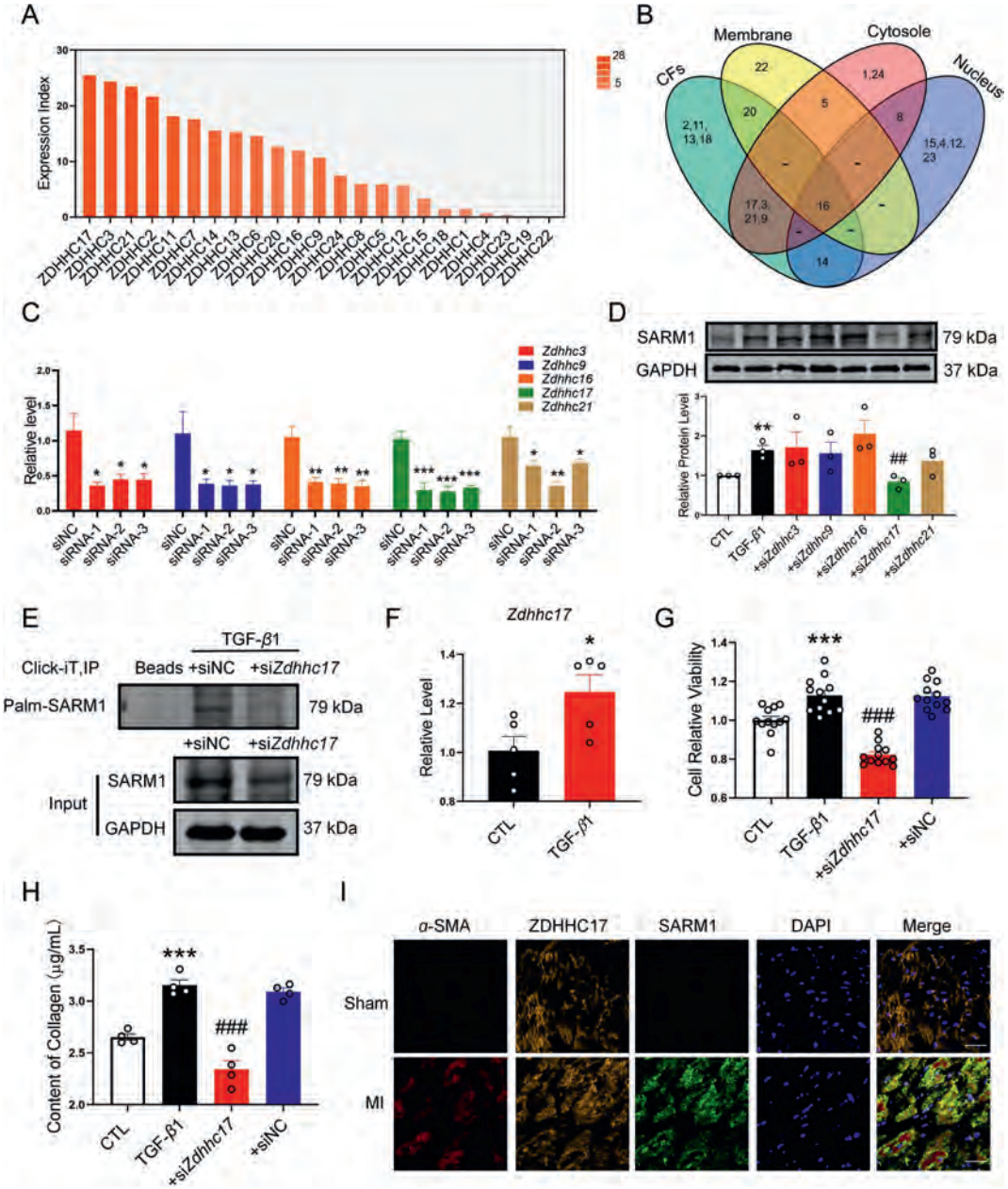

Figure 6 ZDHHC17 mediates palmitoylation of SARM1 in myocardial fibroblasts after MI. (A, B) Venn diagram was used to screen the palmitoyl acylase acting on SARM1 (https://www.proteinatlas.org/). (C) qRT-PCR is used to detect the knockdown efficiency of *Zdhhc3*, *Zdhhc9*, *Zdhhc16*, *Zdhhc17*, and *Zdhhc21*. $n = 4-6$. $^{*}P < 0.05$, $^{**}P < 0.01$, $^{***}P < 0.001$ *vs*. siNC. (D) Western blot was used to detect the protein expression of SARM1 after the deletion of candidate palmitoylase. $n = 3$. $^{**}P < 0.01$ *vs*. CTL, $^{\#\#}P < 0.01$ *vs*. TGF-β1. (E) Click-iT reaction was used to detect the palmitoylation level of SARM1. $n = 3$. (F) qRT-PCR is used to detect the expression of *Zdhhc17* in fibroblasts after TGF-β1 treatment. $n = 5$. $^{*}P < 0.05$ *vs*. CTL. (G) CCK8 to detect the effect of cell viability. $n = 12$. $^{***}P < 0.001$ *vs*. CTL, $^{\#\#\#}P < 0.001$ *vs*. +siNC. (H) The hydroxyproline assay kit is used to detect the secretion of collagen. $n = 4$. $^{***}P < 0.001$ *vs*. CTL, $^{\#\#\#}P < 0.001$ *vs*. +siNC. (I) Multiplex immunohistochemistry is used to detect coexpression between ZDHHC17 and SARM1 in myocardial fibroblasts in the infarct margin area of MI tissue. $n = 3$. Scale bar, 200 μm. Data are presented as mean ± SEM.

of myocardial fibrosis, and we found that selonsertib administration can significantly improve the cardiac function and alleviate collagen deposition in the cardiac tissue (Fig. 8G and H). We tested the protein expression of P4HA1 after administering these two inhibitors. Compared with the MI group, the protein expression of P4HA1 in the heart tissue of mice in the BBC group and selonsertib group was significantly reduced (Supporting Information Fig. S13). By using molecular docking, we found that selonsertib had the great potential to bind with the Glu149, Glu189, Arg224, and Asp317 sites of SARM1, which happens to be the action site of SARM1 and P4HA1 (Supporting Information Fig. S14). The above results suggest that selosertib may be a new anti-cardiac fibrosis candidate by targeting Glu149, Glu189, Arg224, and Asp317 sites of SARM1.

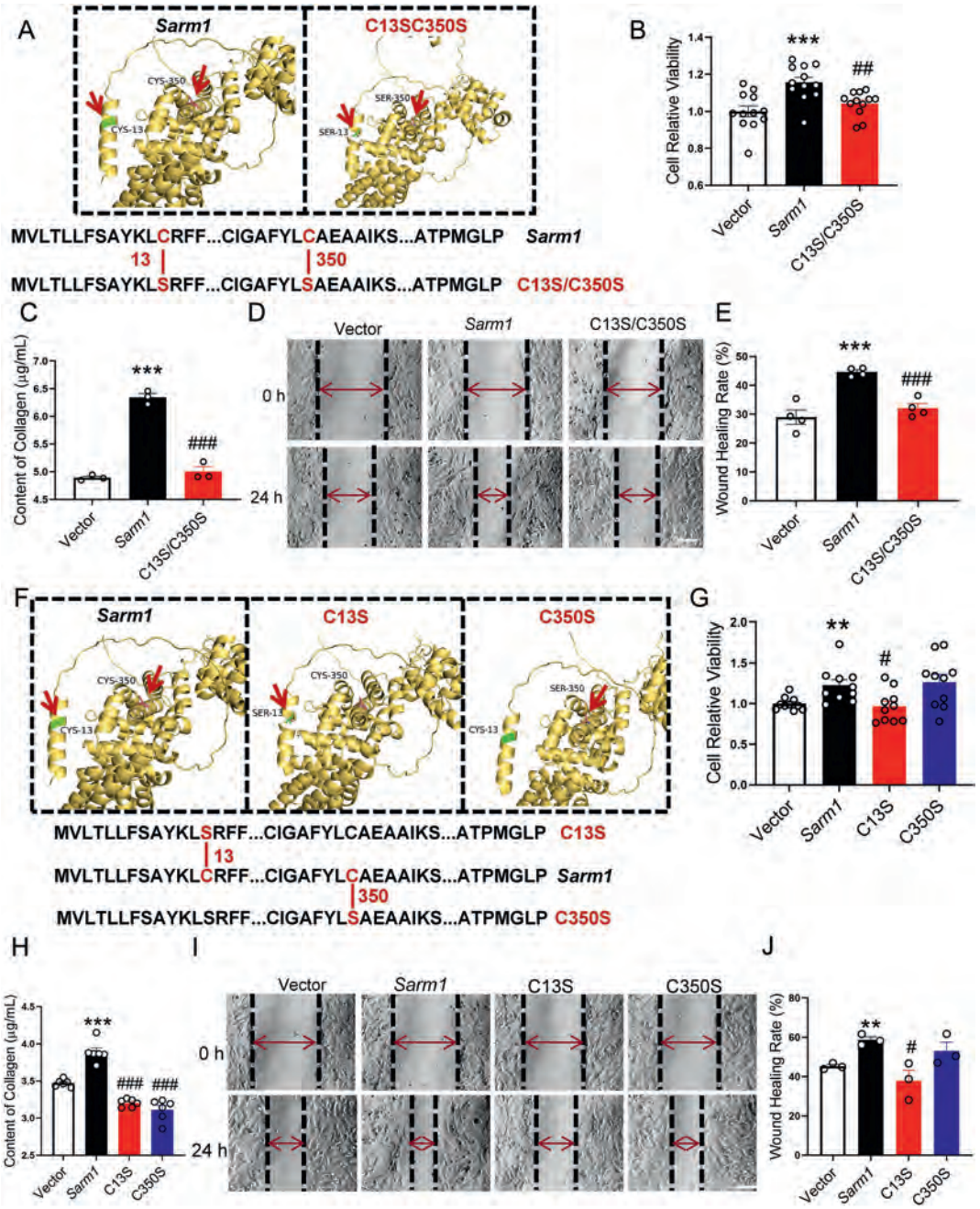

Figure 7 The mutation of SARM1 in the palmitoylation site weakens its role in promoting cardiac fibrosis. (A) The amino acid sequence of C13S/C350S after the SARM1 palmitoylation site (CYS13, CYS350) mutation. (B) CCK8 to detect the effect of cell viability. $n = 12$. $^{***}P < 0.001$ *vs*. Vector, $^{\#\#}P < 0.01$ *vs*. *Sarm1*. (C) The hydroxyproline assay kit is used to detect collagen secretion. $n = 3$. $^{***}P < 0.001$ *vs*. Vector, $^{\#\#\#}P < 0.001$ *vs*. *Sarm1*. (D, E) Wound healing assay to examine the effect of cell migration ability. $n = 4$. $^{***}P < 0.001$ *vs*. Vector, $^{\#\#\#}P < 0.001$ *vs*. *Sarm1*. Scale bar, 100 μm. (F) Amino acid sequences of C13S and C350S after SARM1 palmitoylation site mutation of Cys13 and Cys350, respectively. (G) CCK8 to detect the effect of cell viability. $n = 10$. $^{**}P < 0.01$ *vs*. Vector, $^{\#}P < 0.05$ *vs*. *Sarm1*. (H)The hydroxyproline assay kit is used to detect collagen secretion. $n = 6$. $^{***}P < 0.001$ *vs*. Vector, $^{\#\#\#}P < 0.001$ *vs*. *Sarm1*. (I, J) Wound healing assay to examine the effect of cell migration ability. $n = 3$. $^{**}P < 0.01$ *vs*. Vector, $^{\#}P < 0.05$ *vs*. *Sarm1*. Scale bar, 100 μm. Data are presented as mean ± SEM.

3.9. Sarm1 is associated with cardiac remodeling related diseases and tumors in humans

The data in Fig. 1A demonstrated that the abnormal expression of *Sarm1* was correlated with ICM and DCM. To further explore the possibility of SARM1 as a target for treating human heart disease, we performed the volcano plot analysis of high-throughput sequencing from 3 normal and 3 myocardial infarcted human organoids (GSE115031). As shown in Fig. 8J, the expression of *Sarm1* was significantly increased in infarct organoids, which suggests that *Sarm1* has the potential to be a therapeutic target for myocardial ischemia-related diseases. Our present data suggested

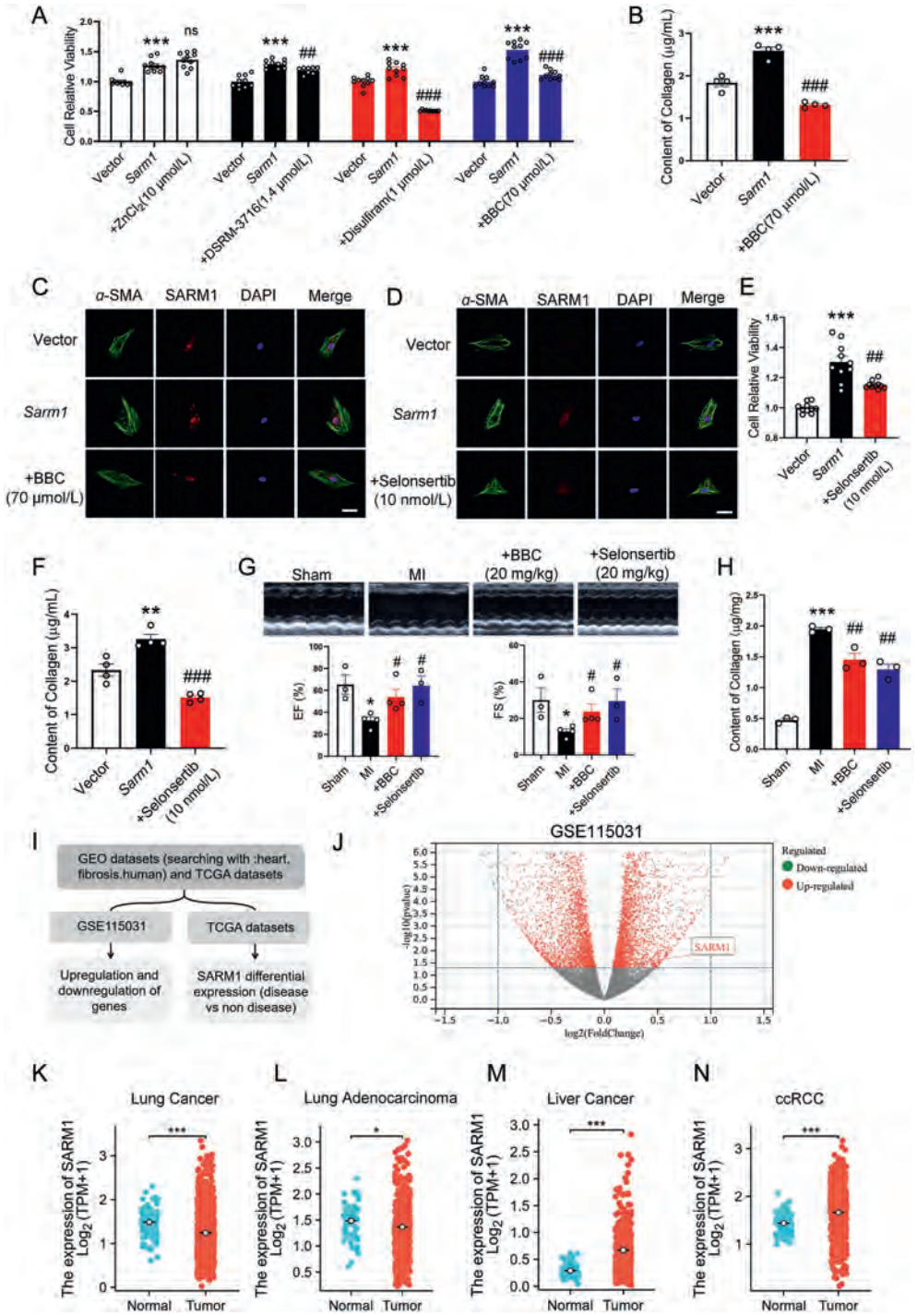

Figure 8 Screening of anti-cardiac fibrosis drugs targeting SARM1. (A) CCK8 was used to detect the effects of disulfiram, BBC, DSRM-3716, and $ZnCl_2$ on cell viability. $n = 10$. $^{***}P < 0.001$ *vs*. Vector, $^{\#\#}P < 0.01$, $^{\#\#\#}P < 0.001$ *vs*. *Sarm1*. (B) The hydroxyproline assay kit was used to detect the secretion of fibroblast collagen by BBC. $n = 4$. $^{***}P < 0.001$ *vs*. Vector, $^{\#\#\#}P < 0.001$ *vs*. *Sarm1*. (C, D) Immunofluorescence in the determination of fibroblast expression of SARM1. $n = 3$. Scale bar, 400 μm. (E) CCK8 to detect the effect of cell viability. $n = 10$. $^{***}P < 0.001$ *vs*. Vector, $^{\#\#}P < 0.01$ *vs*. *Sarm1*. (F) The hydroxyproline assay kit is used to detect collagen secretion. $n = 4$. $^{**}P < 0.01$ *vs*. Vector, $^{\#\#\#}P < 0.001$ *vs*. *Sarm1*. (G) Echocardiographic detection of cardiac function changes. $n = 3$–4. $^{*}P < 0.05$ *vs*. Sham, $^{\#}P < 0.05$ *vs*. MI. (H) The hydroxyproline assay kit is used to detect the secretion of collagen in mouse heart tissue. $n = 3$. $^{***}P < 0.001$ *vs*. Sham, $^{\#\#}P < 0.01$ *vs*. MI. (I) The flowchart of the bioinformatics analysis. (J)Volcano plot of GSE115031. (K−N) TCGA database analyzed the expression of SARM1 in different cancers. $^{*}P < 0.05$, $^{***}P < 0.001$ *vs*. Normal. Clear cell renal cell carcinomas (ccRCCs). Data are presented as mean ± SEM.

that SARM1 knockdown has a protective effect on preventing myocardial fibrosis, and targeted inhibition of SARM1 is a potential strategy for the treatment of myocardial fibrosis. Whether SARM1 is tumorigenic in drug development is the core issue to determine whether it can be an effective drug target. To clarify this issue, we analyzed the expression of *Sarm1* in different cancers by using the TCGA database (Fig. 8I). The results in Fig. 8K−N showed that the expression of *Sarm1* was significantly increased in several types of cancer including lung cancer, liver cancer, and renal cell carcinoma. Moreover, the RNAseq results (GSE216326, GSE217654) from the GEO dataset showed that the expression of *Sarm1* was also significantly increased in a liver injury fibrosis model induced by thioacetamide (TAA) and the mouse renal interstitial fibrosis model (UUO) (Supporting Information Fig. S15).

4. Discussion

Myocardial fibrosis is a common pathological feature of many cardiovascular diseases, including myocardial hypertrophy, heart failure, dilated cardiomyopathy, and diabetic cardiomyopathy[43-46]. The abundance of interstitial and fibroblast cells in the adult heart plays a crucial role in poor repair and fibrosis after MI. Appropriate fibroblast activation and addition can maintain the structural integrity of the heart and partial cardiac function, but fibrosis is often in a state of runaway control. Excessive fibrosis leads to the accumulation of extracellular matrix and fibrosis scarring, resulting in diastolic dysfunction, which is devastating to the recovery of heart function after MI[36,37]. Fibrosis after MI is a key factor affecting the clinical prognosis of patients, which is an urgent problem to be solved[38,47]. In this study, we identified the key fibrotic protein SARM1 as up-regulated after MI.

Previously, researchers had found that SARM1 is the key molecular player involved in the program of axon degeneration[9,19,48]. These advances suggest that SARM1 has potential as a target for therapeutic drugs. In our study, we evaluated the therapeutic role of disulfiram, BBC, 5-iodoisoquinoline (DSRM-3716), zinc chloride ($ZnCl_2$), and selonsertib in myocardial fibrosis. Our data demonstrated that BBC showed anti-fibrosis effects *via* targeting SARM1 palmitoylation sites, while selonsertib interfered with the action site of SARM1 and P4HA1 to inhibit cardiac fibrosis.

The role of SARM1 in cardiovascular disease is not quite clear. In this study, we found that SARM1 participated in the regulation of cardiac fibrosis *via* targeting P4HA1. Proline hydroxylation is an important rate-limiting step in collagen synthesis. It is catalyzed by collagen prolyl 4-hydroxylase (C−P4Hs) and is essential for collagen maturation and secretion. It is related to the occurrence and development of various cancers[49-51]. Xue et al.[52] have shown that HIF-1α can affect the expression of P4HA1 in breast cancer cells through integrin/FAK pathway by targeting Kindlin-2, thus affecting the generation of collagen, thus affecting the stiffness of cancer tissue and promoting cancer metastasis. Shi et al.[53] showed that cycloheximide (CHX) promoted the maturation of type I collagen mainly through P4HA2. In contrast, ascorbic acid and superoxide induce type I collagen maturation mainly through P4HA1 and P4HA1/2. However, whether P4HA1 affects the maturation of different types of collagens in myocardial fibroblasts remains to be further investigated. In addition, the protein expression of P4HA1 increased significantly after TGF-β1 administration. Whether SARM1 mediated its degradation process or participated in the transcription process of P4HA1 remains to be further investigated. However, there is no doubt that P4HA1 mediates the maturation and secretion of collagen. Therefore, the development of specific P4HA1 inhibitors is a promising therapeutic target for the treatment of cardiac fibrosis.

As we prepared for this study, Lee's team[54] constructed a global SARM1 knockout mice to investigate the role of SARM1 in mouse hearts. The collagen levels in the hearts of male KO mice were slightly but significantly elevated, and they believed that this was related to an increase in the number of changes in inflammatory genes related to fibrosis and aging. This is an exciting discovery. This leads us to consider whether SARM1 participates in the development of fibrosis after MI by promoting the expression of inflammation related genes during the inflammatory phase of MI. This also indicates that in the future, it is very important to analyze the role of SARM1 in the inflammatory phase of MI. However, recent studies have shown that SARM1 inhibits the progression of liver fibers by affecting the secretion of inflammatory factors[55]. In this study, the inflammatory process after MI was not discussed, but a large number of research results show that the initial stage after MI (1−7 days) is the inflammatory stage, in which immune cells are activated in large numbers and inflammatory factors are secreted to promote recruitment of all kinds of immune cells to the injured area, but in the later stage of MI is the repair stage. In addition, the detection time involved in our experiment is in the later repair stage. The effect of SARM1 on immune cells in the inflammatory stage after MI is still an important research content that should not be ignored. In the next trial phase, we will further explore the content of this part and continue to improve the important role of SARM1 in various stages after MI. In addition, regarding the drug application of SARM1 as a therapeutic target for various nerve injuries in the field of neurology, the impact of drugs on heart disease cannot be ignored. Our research has a good reference value in this regard. Finally, we screened the antifibrotic effects of SARM1 inhibitors that have been reported so far. This is of great significance for the clinical treatment of anti-fibrosis. In the next step, we will further conduct pharmacodynamics and pharmacokinetics studies in normal mice and transgenic mice, so as to compare with the current drugs in clinical use, and to clarify the effects of the drugs.

It should be noted that there are limitations in the present study. First, the animal models of myocardial fibrosis are relatively limited. Subsequently, we will verify the regulatory effect of SARM1 on myocardial fibrosis in other types of animals, such as rats, using ligation of transverse aortic constriction or isoprenaline-induced myocardial fibrosis model animals. Second, the potential anti-myocardial fibrosis drugs targeted by SARM1, including BBC and selonsertib, have not been validated *in vivo* mice models. We will continue the pharmacodynamics study of BBC and selonsertib against myocardial fibrosis. In addition, BBC may have the problem of poor oral absorption, which will be improved through structural modifications.

5. Conclusions

In summary, we have investigated the effects of SARM1 on ischemia-associated fibrosis in hearts and demonstrated that ZDHHC17 mediated palmitoylation of SARM1 under hypoxia. Moreover, upregulated SARM1 directly acts on P4HA1, promoting extracellular matrix deposition. This study not only fills the research gap of SARM1 in myocardial ischemia but also provides

a reference for the effects of SARM1 inhibitors on the heart in patients with neurological diseases accompanied by ischemic cardiomyopathy. Meanwhile, the inhibition of SARM1 by drugs such as BBC and selonsertib may have therapeutic potential for alleviating ischemic cardiac fibrosis. Our findings demonstrate that targeting SARM1 may be a potential strategy for ischemia-associated and chronic cardiac remodeling.

Acknowledgments

This work was supported by grants from the National Natural Science Foundation of China (82370417, 82270273, 82330011, and U21A20339), Heilongjiang Province National Science Fund for Distinguished Young Scholars (JQ2024H001, China), CAMS Innovation Fund for Medical Sciences (2020-I2M-5-003, China).

Author contributions

Xuewen Yang: Validation, Formal analysis, Writing − original draft, Conceptualization, Methodology, Writing − review & editing, Data curation, Visualization. Yanwei Zhang: Visualization. Xiaoping Leng: Conceptualization. Yanying Wang: Data curation. Manyu Gong: Validation. Dongping Liu: Validation. Haodong Li: Validation. Zhiyuan Du: Data curation. Zhuo Wang: Validation. Lina Xuan: Conceptualization. Ting Zhang: Conceptualization. Han Sun: Visualization. Xiyang Zhang: Visualization. Jie Liu: Validation. Tong Liu: Visualization. Tiantian Gong: Visualization. Zhengyang Li: Visualization. Shengqi Liang: Investigation. Lihua Sun: Methodology. Lei Jiao: Funding acquisition, Writing − review & editing, Conceptualization. Baofeng Yang: Funding acquisition, Conceptualization. Ying Zhang: Supervision, Funding acquisition.

Conflicts of interest

The authors declare no competing interests.

Appendix A. Supporting information

Supporting information to this article can be found online at https://doi.org/10.1016/j.apsb.2025.07.011.

References

1. Chalise U, Becirovic-Agic M, Lindsey ML. The cardiac wound healing response to myocardial infarction. *WIREs Mech Dis* 2023;**15**: e1584.
2. Jenca D, Melenovsky V, Stehlik J, Stanek V, Kettner J, Kautzner J, et al. Heart failure after myocardial infarction: incidence and predictors. *ESC Heart Fail* 2021;**8**:222−37.
3. Groenewegen A, Rutten FH, Mosterd A, Hoes AW. Epidemiology of heart failure. *Eur J Heart Fail* 2020;**22**:1342−56.
4. Chen J, Wei X, Zhang Q, Wu Y, Xia G, Xia H, et al. The traditional Chinese medicines treat chronic heart failure and their main bioactive constituents and mechanisms. *Acta Pharm Sin B* 2023;**13**:1919−55.
5. Zaidi Y, Aguilar EG, Troncoso M, Ilatovskaya DV, DeLeon-Pennell KY. Immune regulation of cardiac fibrosis post myocardial infarction. *Cell Signal* 2021;**77**:109837.
6. Scalise RFM, De Sarro R, Caracciolo A, Lauro R, Squadrito F, Carerj S, et al. Fibrosis after myocardial infarction: an overview on cellular processes, molecular pathways, clinical evaluation and prognostic value. *Med Sci* 2021;**9**:16.
7. Chen G, Xu H, Xu T, Ding W, Zhang G, Hua Y, et al. Calycosin reduces myocardial fibrosis and improves cardiac function in post-myocardial infarction mice by suppressing TGFBR1 signaling pathways. *Phytomedicine* 2022;**104**:154277.
8. Dolivo D, Weathers P, Dominko T. Artemisinin and artemisinin derivatives as anti-fibrotic therapeutics. *Acta Pharm Sin B* 2021;**11**: 322−39.
9. McGuinness HY, Gu W, Shi Y, Kobe B, Ve T. SARM1-dependent axon degeneration: nucleotide signaling, neurodegenerative disorders, toxicity, and therapeutic opportunities. *Neuroscientist* 2023;**31**: 473−92.
10. Waller TJ, Collins CA. Multifaceted roles of SARM1 in axon degeneration and signaling. *Front Cell Neurosci* 2022;**16**:958900.
11. Lai MY, Li J, Zhang XX, Wu W, Li ZP, Sun ZX, et al. SARM1 participates in axonal degeneration and mitochondrial dysfunction in prion disease. *Neural Regen Res* 2022;**17**:2293−9.
12. Miao X, Wu Q, Du S, Xiang L, Zhou S, Zhu J, et al. SARM1 promotes neurodegeneration and memory impairment in mouse models of Alzheimer's disease. *Aging Dis* 2023;**25**:390−407.
13. Zhou K, Tan Y, Zhang G, Li J, Xing S, Chen X, et al. Loss of SARM1 ameliorates secondary thalamic neurodegeneration after cerebral infarction. *J Cereb Blood Flow Metab* 2023;**28**:224−38.
14. Figley MD, Gu W, Nanson JD, Shi Y, Sasaki Y, Cunnea K, et al. SARM1 is a metabolic sensor activated by an increased NMN/NAD^+ ratio to trigger axon degeneration. *Neuron* 2021;**109**:1118−36.
15. Angeletti C, Amici A, Gilley J, Loreto A, Trapanotto AG, Antoniou C, et al. SARM1 is a multi-functional NAD(P)ase with prominent base exchange activity, all regulated by multiple physiologically relevant NAD metabolites. *iScience* 2022;**25**:103812.
16. Pan ZG, An XS. SARM1 deletion restrains NAFLD induced by high fat diet (HFD) through reducing inflammation, oxidative stress and lipid accumulation. *Biochem Biophys Res Commun* 2018;**498**:416−23.
17. Yan K, Hou L, Liu T, Jiao W, Ma Q, Fang Z, et al. lncRNA OGFRP1 functions as a ceRNA to promote the progression of prostate cancer by regulating SARM1 level *via* miR-124-3p. *Aging (Albany NY)* 2020;**12**: 8880−92.
18. Bosanac T, Hughes RO, Engber T, Devraj R, Brearley A, Danker K, et al. Pharmacological SARM1 inhibition protects axon structure and function in paclitaxel-induced peripheral neuropathy. *Brain* 2021;**29**: 3226−38.
19. Hughes RO, Bosanac T, Mao X, Engber TM, DiAntonio A, Milbrandt J, et al. Small molecule SARM1 inhibitors recapitulate the $SARM1^{-/-}$ phenotype and allow recovery of a metastable pool of axons fated to degenerate. *Cell Rep* 2021;**34**:108588.
20. Zhao YJ, He WM, Zhao ZY, Li WH, Wang QW, Hou YN, et al. Acidic pH irreversibly activates the signaling enzyme SARM1. *FEBS J* 2021; **288**:6783−94.
21. Loring HS, Parelkar SS, Mondal S, Thompson PR. Identification of the first noncompetitive SARM1 inhibitors. *Bioorg Med Chem* 2020; **28**:115644.
22. Bratkowski M, Xie T, Thayer DA, Lad S, Mathur P, Yang YS, et al. Structural and mechanistic regulation of the pro-degenerative NAD hydrolase SARM1. *Cell Rep* 2020;**32**:107999.
23. Jiao L, Gong M, Yang X, Li M, Shao Y, Wang Y, et al. NAD^+ attenuates cardiac injury after myocardial infarction in diabetic mice through regulating alternative splicing of VEGF in macrophages. *Vascul Pharmacol* 2022;**147**:107126.
24. He Z, Jiao H, An Q, Zhang X, Zengyangzong D, Xu J, et al. Discovery of novel 4-phenylquinazoline-based BRD4 inhibitors for cardiac fibrosis. *Acta Pharm Sin B* 2022;**12**:291−307.
25. Xie S, Xing Y, Shi W, Zhang M, Chen M, Fang W, et al. Cardiac fibroblast heat shock protein 47 aggravates cardiac fibrosis post myocardial ischemia-reperfusion injury by encouraging ubiquitin specific peptidase 10 dependent Smad4 deubiquitination. *Acta Pharm Sin B* 2022;**12**:4138−53.
26. Dong Y, Xu J, Sun B, Wang J, Wang Z. MET-targeted therapies and clinical outcomes: a systematic literature review. *Mol Diagn Ther* 2022;**26**:203−27.

27. Jin J, Zhi X, Wang X, Meng D. Protein palmitoylation and its pathophysiological relevance. *J Cell Physiol* 2021;**236**:3220−33.
28. Zhou B, Hao Q, Liang Y, Kong E. Protein palmitoylation in cancer: molecular functions and therapeutic potential. *Mol Oncol* 2023;**17**: 3−26.
29. Das T, Yount JS, Hang HC. Protein *S*-palmitoylation in immunity. *Open Biol* 2021;**11**:200411.
30. Pham TV, Hsiao WY, Wang YT, Yeh SD, Wang SW. Protein *S*-palmitoylation regulates different stages of meiosis in *Schizosaccharomyces pombe*. *Life Sci Alliance* 2023;**6**:e202201755.
31. Zhao L, Zhang C, Luo X, Wang P, Zhou W, Zhong S, et al. CD36 palmitoylation disrupts free fatty acid metabolism and promotes tissue inflammation in non-alcoholic steatohepatitis. *J Hepatol* 2018;**69**: 705−17.
32. Rech L, Abdellatif M, Pöttler M, Stangl V, Mabotuwana N, Hardy S, et al. Small molecule STING inhibition improves myocardial infarction remodeling. *Life Sci* 2022;**291**:120263.
33. Zhu X, Liu S, Yang X, Wang W, Shao W, Ji T. P4HA1 as an unfavorable prognostic marker promotes cell migration and invasion of glioblastoma *via* inducing EMT process under hypoxia microenvironment. *Am J Cancer Res* 2021;**11**:590−617.
34. Li Y, Ge YZ, Qian Y, Chen K, Zhao F, Qin Z, et al. The role of P4HA1 in multiple cancer types and its potential as a target in renal cell carcinoma. *Front Genet* 2022;**13**:848456.
35. Zhou R, Qiu L, Zhou L, Geng R, Yang S, Wu J. P4HA1 activates HMGCS1 to promote nasopharyngeal carcinoma ferroptosis resistance and progression. *Cell Signal* 2023;**105**:110609.
36. Gou W, Yang Y, Shan Q, Xia S, Ma Y. P4HA1, transcriptionally activated by STAT1, promotes esophageal cancer progression. *Pathol Int* 2023;**73**:147−58.
37. Wu Q, He Y, Liu X, Luo F, Jiang Y, Xiang M, et al. Cancer stem cell-like cells-derived exosomal lncRNA CDKN2B-AS1 promotes biological characteristics in thyroid cancer *via* miR-122-5p/P4HA1 axis. *Regen Ther* 2023;**22**:19−29.
38. Zhu M, Yan T, Zhu S, Weng F, Zhu K, Wang C, et al. Identification and verification of FN1, P4HA1 and CREBBP as potential biomarkers in human atrial fibrillation. *Math Biosci Eng* 2023;**20**:6947−65.
39. Nattel S. Molecular and cellular mechanisms of atrial fibrosis in atrial fibrillation. *JACC Clin Electrophysiol* 2017;**3**:425−35.
40. Weng L, Ye J, Yang F, Jia S, Leng M, Jia B, et al. TGF-β1/SMAD3 regulates programmed cell death 5 that suppresses cardiac fibrosis post-myocardial infarction by inhibiting HDAC3. *Circ Res* 2023;**133**: 237−51.
41. Zhao T, Chen H, Cheng C, Zhang J, Yan Z, Kuang J, et al. Liraglutide protects high-glucose-stimulated fibroblasts by activating the CD36−JNK−AP1 pathway to downregulate P4HA1. *Biomed Pharmacother* 2019;**118**:109224.
42. Harrison SA, Wong VW, Okanoue T, Bzowej N, Vuppalanchi R, Younes Z, et al. STELLAR-3 and STELLAR-4 investigators. Selonsertib for patients with bridging fibrosis or compensated cirrhosis due to NASH: results from randomized phase III STELLAR trials. *J Hepatol* 2020;**73**:26−39.
43. Tuleta I, Frangogiannis NG. Fibrosis of the diabetic heart: clinical significance, molecular mechanisms, and therapeutic opportunities. *Adv Drug Deliv Rev* 2021;**176**:113904.
44. Habib M, Adler A, Fardfini K, Hoss S, Hanneman K, Rowin EJ, et al. Progression of myocardial fibrosis in hypertrophic cardiomyopathy: a cardiac magnetic resonance study. *JACC Cardiovasc Imaging* 2021; **14**:947−58.
45. Li W, Lou X, Zha Y, Qin Y, Zha J, Hong L, et al. Single-cell RNA-seq of heart reveals intercellular communication drivers of myocardial fibrosis in diabetic cardiomyopathy. *eLife* 2023;**12**:e80479.
46. Cheng Y, Wang Y, Yin R, Xu Y, Zhang L, Zhang Y, et al. Central role of cardiac fibroblasts in myocardial fibrosis of diabetic cardiomyopathy. *Front Endocrinol (Lausanne)* 2023;**14**:1162754.
47. Xu LY, Xie L, Wang J, Chen HX, Cai HL, Tian LJ, et al. Correlation between serum laminin levels and prognosis of acute myocardial infarction. *Front Cardiovasc Med* 2022;**9**:936983.
48. Wang S, Zhang Y, Lou J, Yong H, Shan S, Liu Z, et al. The therapeutic potential of berberine chloride against SARM1-dependent axon degeneration in acrylamide-induced neuropathy. *Phytother Res* 2023; **37**:77−88.
49. Robinson AD, Chakravarthi BVSK, Agarwal S, Chandrashekar DS, Davenport ML, Chen G, et al. Collagen modifying enzyme P4HA1 is overexpressed and plays a role in lung adenocarcinoma. *Transl Oncol* 2021;**14**:101128.
50. Sato K, Sano D, Takahashi H, Kuwahara T, Aizawa Y, Aoyama J, et al. P4HA1 promotes cell migration and colonization in hypopharyngeal squamous cell carcinoma. *Anticancer Res* 2023;**43**:2571−82.
51. Zhou Y, Tian J, Zhu Y, Zhang Y, Zhao X. Multilevel chitosan-gelatin particles loaded with P4HA1 siRNA suppress glioma development. *Drug Deliv Transl Res* 2024;**3**:665−77.
52. Xue X, Xue S, Wan W, Li J, Shi H. HIF-1α interacts with Kindlin-2 and influences breast cancer elasticity: a study based on shear wave elastography imaging. *Cancer Med* 2020;**9**:4971−9.
53. Shi R, Xu M, Ye H, Gao S, Li J, Li H, et al. Cycloheximide promotes type I collagen maturation mainly *via* collagen prolyl 4-hydroxylase subunit α2. *Acta Biochim Biophys Sin* 2022;**54**:1832−40.
54. Nizami HL, Minor KE, Chiao YA, Light CM, Lee CF. Sexually dimorphic effects of SARM1 deletion on cardiac NAD^+ metabolism and function. *Am J Physiol Heart Circ Physiol* 2022;**323**:H774−81.
55. Tao L, Yang G, Sun T, Jie Tao, Zhu C, Yu H, et al. Capsaicin receptor TRPV1 maintains quiescence of hepatic stellate cells in the liver *via* recruitment of SARM1. *J Hepatol* 2023;**78**:805−19.